SAGE III/ISS aerosol/cloud categorization and its impact on GloSSAC

Mahesh Kovilakam[1,2], Larry W. Thomason[2], and Travis Knepp[2]

[1]SSAI, Hampton, Virginia, USA

[2]NASA Langley Research Center, Hampton, Virginia, USA

Correspondence: Mahesh Kovilakam (mahesh.kovilakam@nasa.gov)

Abstract. The Stratospheric Aerosol and Gas Experiment on the International Space Station (SAGE III/ISS) began its mission in June 2017. SAGE III/ISS is an updated version of the SAGE III on Meteor (SAGE III/M3M) instrument ~~that~~ and makes observations of stratospheric aerosol extinction coefficient at wavelengths that range from 385 to 1550 nm with a near global coverage between 60°S and 60°N. While SAGE III/ISS makes reliable and robust solar occultation measurements in the stratosphere, similar to its predecessors, interpreting aerosol extinction measurements in the vicinity of the tropopause and in the troposphere have been a challenge for all SAGE instruments because of the potential for cloud interference. Herein, we discuss some of the challenges associated with discriminating between aerosols and clouds within the extinction measurements and describe the methods implemented to categorize clouds and aerosols using available SAGE III/ISS aerosol measurements. This cloud/aerosol categorization method is based on the results of Thomason and Vernier (2013) with some modifications that now incorporate the influence of recent volcanic/PyroCb events~~and a new method of locating aerosol centroid based on k-medoid clustering. We use version 5.2 of SAGE III~~. Herein we describe this new cloud/~~ISS extinction coefficients for the analysis. The current algorithmnow classifies standard (background) and non-standard (enhanced) aerosols in the stratosphere and identify enhanced aerosols and~~ aerosol categorization algorithm, demonstrate how it identifies enhanced aerosols and aerosol/-cloud mixture in the ~~tropopause region. SAGE data is an important dataset in the GloSSAC data base and therefore,~~ lower stratospheric region, and discuss the impact of ~~cloud-filtered aerosol extinction coefficient measurements~~ this cloud-filtering algorithm on the latest ~~version of GloSSAC (version 2.2) is also discussed.~~ release of the Global Space-based Stratospheric Aerosol Climatology (GloSSAC) dataset.

1 Introduction

~~The Stratospheric Aerosol and Gas Experiment on the International Space Station (SAGE III/ISS) began collecting data in June 2017 and is an updated version of the SAGE III on Meteor (SAGE III/M3M) instrument. SAGE III/ISS works similar to its predecessors (e.g. Mauldin et al., 1985; Thomason et al., 2010)0pt, retreiving vertical profiles of multi-wavelength aerosol extinction coefficient (384, 449, 521, 602, 676, 756, 869, 1022, and 1544 nm) along with other gaseous measurements such as ozone (O_3), water vapor (H_2O), and Nitrogen dioxide (NO_2) using solar occultation technique. The SAGE family of instruments have been instrumental in providing vertical profiles of global stratospheric aerosol that have been used by various correlative~~

measurements for comparison and validation purposes (e.g. Hervig and Deshler, 2002; Deshler et al., 2003, 2019; Rieger et al., 2019; Bour
Further, the SAGE series of measurements have been used for providing a global space-based stratospheric aerosol climatology
(GloSSAC) with other space-based measurements (Thomason et al., 2018; Kovilakam et al., 2020)0pt.

Several studies have shown the importance of the impact of stratospheric aerosols on The importance of stratospheric aerosol in determining the energy balance of the atmosphere (e.g. Hofmann and Solomon, 1989; Fahey et al., 1993; Minnis et al., 1993)0pthas been well documented (e.g. Hofmann and Solomon, 1989; Fahey et al., 1993; Minnis et al., 1993; Kloss et al., 2021; Sellitto et al., 2022a, Recent years have witnessed frequent small to moderate volcanic eruptions and wildfireas well as wildfire/pyrocumulonimbus (PyroCb) events that injected aerosols into the stratosphere, which resulted in radiative, chemical, and dynamical impact in the stratosphere (Peterson et al., 2018; Yu et al., 2019; Kablick III et al., 2020; Knepp et al., 2021)0pt(Peterson et al., 2018; Yu et al., 2019; K Additionally, studies have shown that relatively low aerosol loading smaller aerosol perturbations can also have radiative impact in the stratosphere (Vernier et al., 2011). It is therefore important to get Therefore, having accurate information of stratospheric aerosol extinction during and following such events and to have the ability to distinguish between aerosol aerosols associated with these events and clouds is highly important. The objective of this study was is to develop an aerosol-cloud separation algorithm that enables this distinction under perturbed conditions following events such as volcanic eruptions and Pyrocumulonimbus (PyroCb) PyroCb events.

Several cloudand Previous cloud/aerosol discrimination studies have been documented in the past using SAGE data (e.g. Kent and McCor These studies have one thing in common, which is the usage (e.g. Kent and McCormick, 1991; Kent et al., 1993; Wang et al., 1994; Kent et on the use of multi-wavelength SAGE extinction coefficient measurements to infer information about particle sizessize. Kent et al. (1993) developed a method to separate aerosol and clouds using an extinction coefficient distribution based on SAGE II measurements at 525 and 1020 nm. A key finding of Kent et al. (1993) was that optically thin clouds are in fact aerosol-cloud mixtures and they concluded that the transition from aerosol to aerosol/cloud occurs over a continuum. Wang et al. (1994) later investigated aerosol-cloud interaction of tropical high clouds using the same wavelength combination as Kent et al. (1993), but with additional information of temperature to identify the presence of high clouds in the tropical region. A different approach using three wavelength combinations (525, 1020, and 1550 nm) was later developed by Kent et al. (1997a) for SAGE II-I/M3M to identify cloud height. While studies show differences in identifying tropopause height between different re-analyses (e.g. Boothe and Homeyer, 2017; Manney et al., 2017; Xian and Homeyer, 2019)0pt, accurate estimation of tropopause height is an important factor in identifying clouds in the vicinity of tropopause, so as to not bias aerosol data.

Herein, we describe a cloud screening algorithm for SAGE III/ISS to study the challenges in identifying pure aerosol and aerosol-cloud mixture from SAGE III/ISS observations and their impact on the development of GloSSAC version 2.2 the latest version of GloSSAC (v2.2). It is worthwhile to note here that the aerosol record post-2017 witnessed several volcanic eruptions and wildfire events that injected particles into the stratosphere, further complicating the separation of aerosol and clouds near the tropopause. As previously noted, Thomason and Vernier (2013) (hereafter TV13) have studied the challenges in separating aerosol and cloud using used SAGE II observations particularly during from a volcanically quiescent period for the (1999-2005) to study the challenges in separating aerosol and cloud within the tropical Upper Troposphere and Lower Stratosphere (UTLS) region. For SAGE IIIThis discrimination becomes more challenging when the UTLS is perturbed by

volcanic and/~~ISS, it becomes even more challenging due to frequent moderate volcanic eruptions andwildfire events that occurred during~~ or pyroCb activity, such as during the SAGE III/ISS ~~measurements. Here~~data record. Herein, we describe a modified ~~version of~~ TV13 ~~to account for the perturbed events, thereby implementing the method not only for the tropics but for the entire global dataset~~(hereafter TV13*) to accommodate SAGE III/ISS measurements and to facilitate comparisons with a new method developed specially for the complex environment observed during the SAGE III/ISS mission (SAGE III/ISS Operational Aerosol Type Classification Method (hereafter SOATCM)), which is based on TV13* that is applicable at all latitudes (i.e., not just the tropics as in TV13) and does not rely on quiescent conditions.

1.1 ~~SAGE III/ISS muti-wavelength extinction measurements and version changes~~

2 Data

~~A newer version (version 5.2) of SAGE~~ The Stratospheric Aerosol and Gas Experiment on the International Space Station (SAGE III/ISS) began collecting data in June 2017 and is an updated version of the SAGE III on Meteor (SAGE III/M3M) instrument. SAGE III/ISS works similar to its predecessors (e.g. Mauldin et al., 1985; Thomason et al., 2010)0pt, retrieving vertical profiles of multi-wavelength aerosol extinction coefficient (384, 449, 521, 602, 676, 756, 869, 1022, and 1544 nm) in addition to gas-phase species. The SAGE family of instruments have a heritage of providing high-precision (<5%) vertical profiles of global stratospheric aerosol that has been used by various correlative measurements for comparison and validation purposes (e.g. Hervig and Deshler, 2002; Deshler et al., 2003, 2019; Rieger et al., 2019; Bourassa et al., 2019) 0pt. Further, the SAGE series of measurements have been used for providing a global space-based stratospheric aerosol climatology (GloSSAC) with other space-based measurements (Thomason et al., 2018; Kovilakam et al., 2020)0pt.

We use SAGE III/ISS ~~data is recently released~~(version 5.2) data for all the analyses described in this paper. The changes ~~occurred~~ introduced in version 5.2 are described in the version 5.2 release notes (https://sage.nasa.gov/wp/wp-content/uploads/2021/07/SAGEIII_Release_Notes_v5.2.pdf). Some of the broad changes in the solar product in version 5.2 includes non-smoothing of solar data products, altitude registration correction and an automated "QA" process. While SAGE III/ISS aerosol extinction measurements have been used for validation, comparison and long-term climatology purposes (e.g. Bourassa et al., 2019; Rieger et al., 2019; Kar et al., 2019; Kovilakam et al., 2020), a negative bias in the aerosol channels (521, 602, and 676 nm) close to ~~Chappius band has been recently noted (Wang et al., 2020) 0pt~~the Chappuis ozone absorption band is present in the v5.2 aerosol data (Wang et al., 2020) 0ptand caution must be used in using those aerosol extinction coefficient measurements. This reported bias is currently being investigated.

3 Methods

3.1 Screening of SAGE III/ISS Negative Extinction Coefficients

SAGE III/ISS makes measurement similar to SAGE II up to a line-of-sight (LOS) optical depth close to 7. We, therefore follow the TV13 method to first terminate each profile at the ~~first altitudeat which~~ highest altitude, where aerosol extinction exceeds 2 X10^{-2} km^{-1} or the LOS optical depth (LOS OD) exceeds 7.

For SAGE III/ISS version 5.2, we notice that some profiles report negative extinction coefficients in the UTLS. ~~Due to the noise characteristics of the SAGE III/ISS transmission data , some SAGE III/ISS profiles have significant noise in them that can lead to product uncertainties that do not satisfactorily account for this negative retrieval. For example,~~ Normally, these negative values occur at higher altitudes, which is not unexpected, or have uncertainties that are large enough to make the extinction coefficients effectively indistinguishable from zero. For higher altitudes ($\geq$ 25 km), negative values mostly occur due to noise and errors in the removal of ozone and molecular scattering and therefore all data above 25 km were retained. Below 25 km, negative values in the extinction coefficient most commonly occur below very dense layers like clouds and uncertainties reflect that these data are of low quality. However, we observe some situations where negative values occur with uncertainties that suggest that they are reasonable. Figure 1a demonstrates this phenomenon in the UTLS with the color-coded dots indicating the relative uncertainty (extinction coefficients were plotted as absolute values to accommodate the log scale). ~~Here, it was observed that two points had negative extinction coefficieints, but had relative uncertainties less than 50%. Normally, these negative values occur at higher altitudes, which is not unexpected, or have uncertainties that are large enough to make the extinction coefficients effectively indistinguishable from zero. However, that is not what was observed for the points in Figure 1a. This phenomenon seems to occur predominantly in the vicinity of a large positive extinction coefficient , particularly~~ This negative extinction coefficient issue occurs between 12 and 14 km in Figure 1~~. Because of the inherent sensitivity in separating clouds and aerosols in occultation-type data, we developed a filtering algorithm to mitigate the influence of these negative extinction coefficients on subsequent analyses. This filtering algorithm scans for negative values from the top of the profile downward, starting at an altitude of 25 km down to where the profile terminates. For higher altitudes ($\geq$ 25 km) , negative values mostly occur due to noise and errors in the removal of ozone and molecular scattering, therefore higher altitude negative extinction coefficients are retained. However, when they occur at lower altitudes particularly in the vicinity of tropopause or below is~~ a with a large aerosol extinction (1.37x10^{-2} km^{-1}) at 13 km and a ~~sign that the measurements are less reliable. Therefore, the screening algorithm is hard coded to terminate profiles just above the altitude where the first negative value occurs in the troposphere. However, the algorithm is more selective on how data are removed within the stratosphere. For example, when a~~ negative ~~extinction coefficient was observed in the stratosphere the data points at adjacent altitudes (i. e., the altitude immediately above and below the negative value) were removed from the data set; resulting on only 3 data points being removed. However, when a negative extinction coefficient was observed in the troposphere that data point as well as all data points below it were removed. This filtering mechanism can be seen at work~~ aerosol extinction (-2.94x10^{-3} km^{-1}) at 12 km with an uncertainty of less than 50%. For SAGE like solar occultation measurements, it is likely that a negative extinction value is reported below a large positive one because of the retrieval assumption of atmospheric homogeneity.

SAGE measurements of transmission at a given altitude are the average of multiple line-of-sight (LOS) measurements and the average value of these samples transmission is used in the retrieval of all science products and strict homogeneity is assumed (Thomason et al., 2003)0pt. It is likely that these apparently significant negative extinction coefficient values are due to a breakdown of the horizontal homogeneity assumed by the data processing. In this case, it is likely that the LOS optical depth at 13 km is comprised of at least some observations of a dense layer at 13 km that produces a high average optical depth for this altitude. Conversely, at the altitudes immediately below the 13 km layer, the LOS observations must miss the layer at 13 km entirely, see it less frequently, or see much less dense parts of it and thus produce a relatively low average LOS optical depth. To the retrieval algorithm, the only solution is to produce a big negative extinction value at 12 km to compensate for the large value at 13 km. Since these values are particularly difficult to handle, given the negative extinction but low uncertainty, we have developed a filtering process to identify and eliminate these data, which is outlined in Figure ~~1b where three points were removed around 11 km and all data below6.5 km were removed.~~ 2 and is described below:

4 ~~Aerosol and Cloud identification in SAGE III/ISS observations~~

~~Several previous studies (e.g. Thomason et al., 2008; Thomason and Vernier, 2013) 0pthave provided in depth analyses of multi-wavelengt stratospheric aerosol extinction coefficients from SAGE II and how extinction ratios relate to the particle sizes on the basis of Mie theory. Theoretically,~~

- We use SAGE III/ISS level 2 version 5.2 aerosol extinction coefficient data (k(z), where k is the extinction coefficient at altitude "z") as shown in Figure 2 (a).
- As a first step, the algorithm searches for the altitude (z) , where k(z) exceeds 2 $X10^{-2}$ km^{-1} or the LOS optical depth (LOS OD) exceeds 7 (see Figure 2(b)).
- If the criterion shown in Figure 2(b) is "True" (Figure 2(c)), then we set all extinction (k(z)) values below the altitude "z" to missing as shown in Figure 2(d).
- As a next step, we identify tropopause altitude ($trp_{(z)}$) (Figure 2(e)).
- The filtering algorithm then scans for negative values ($k_{n(z)}$) from the top of the profile downward, starting at an altitude of 25 km down to where the profile terminates based on tropopause altitude (Figure 2(f)).
- In the next step (Figure 2(g)), the extinction profile is divided based on tropopause height ($trp_{(z)}$).
- If the negative extinction value ($k_{n(z)}$) is above $trp_{(z)}$, then the algorithm set the data points at adjacent altitudes (i.e., the altitude immediately above ($k_{n(z-1)}$) and below ($k_{n(z+1)}$) the negative value) including the negative extinction value ($k_{n(z)}$) to missing values (Figure 2 (h)). The screening of these values can be seen in the sample extinction profile (between 12 and 14 km) in Figure 1b.

– If the negative extinction value ($k_{n(z)}$) is observed below $trp_{(z)}$, then the algorithm set all data below $k_{n(z+1)}$ to missing values (Figure 2 (i)). This filtering mechanism can be seen at work in Figure 1b, where all data below 6.5 km were removed.

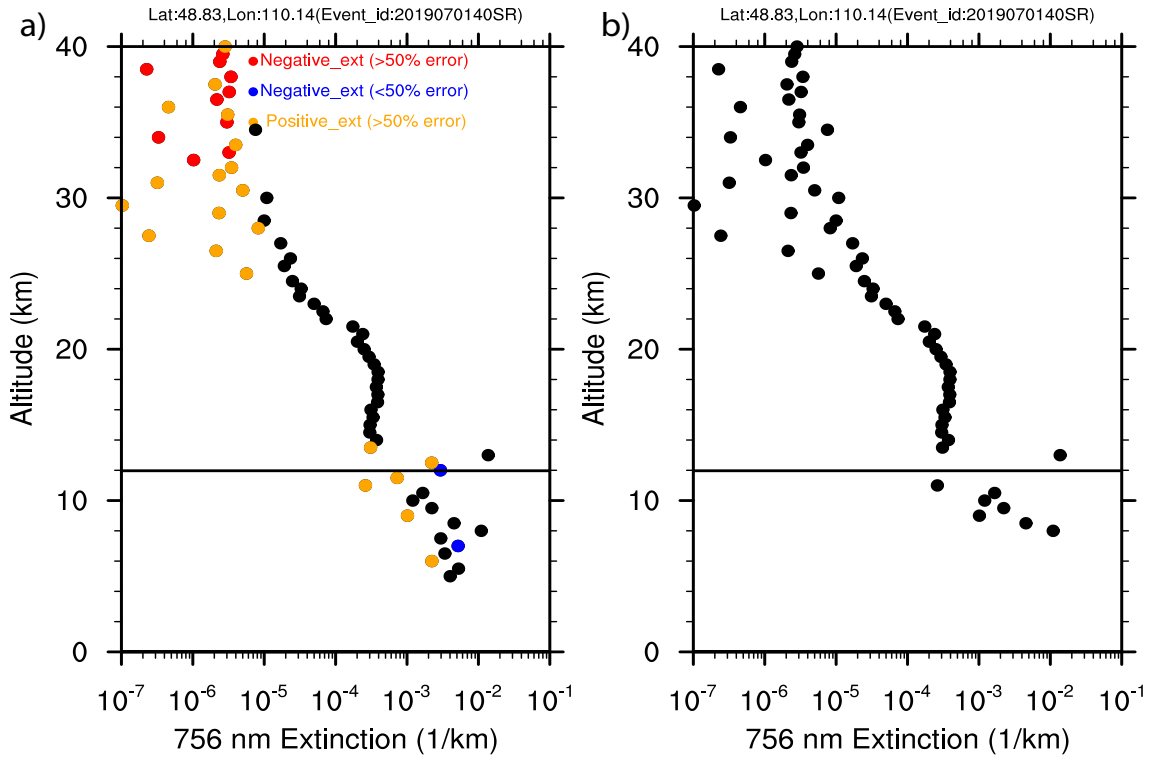

Figure 1. A sample extinction profile at 756 nm that shows negative extinction values in the lower stratosphere as well as in the troposphere (Left). All extinction values are plotted as absolute values and negative extinction values are color coded using red (blue) filled circles with $> 50\%$ ($< 50\%$) error, whereas orange symbols represent positive extinction with $> 50\%$ error. The right panel shows the absolute extinction profile after filtering negative values. The absolute value of the negative extinction coefficients (blue and red dots) are plotted to accommodate the log scale.

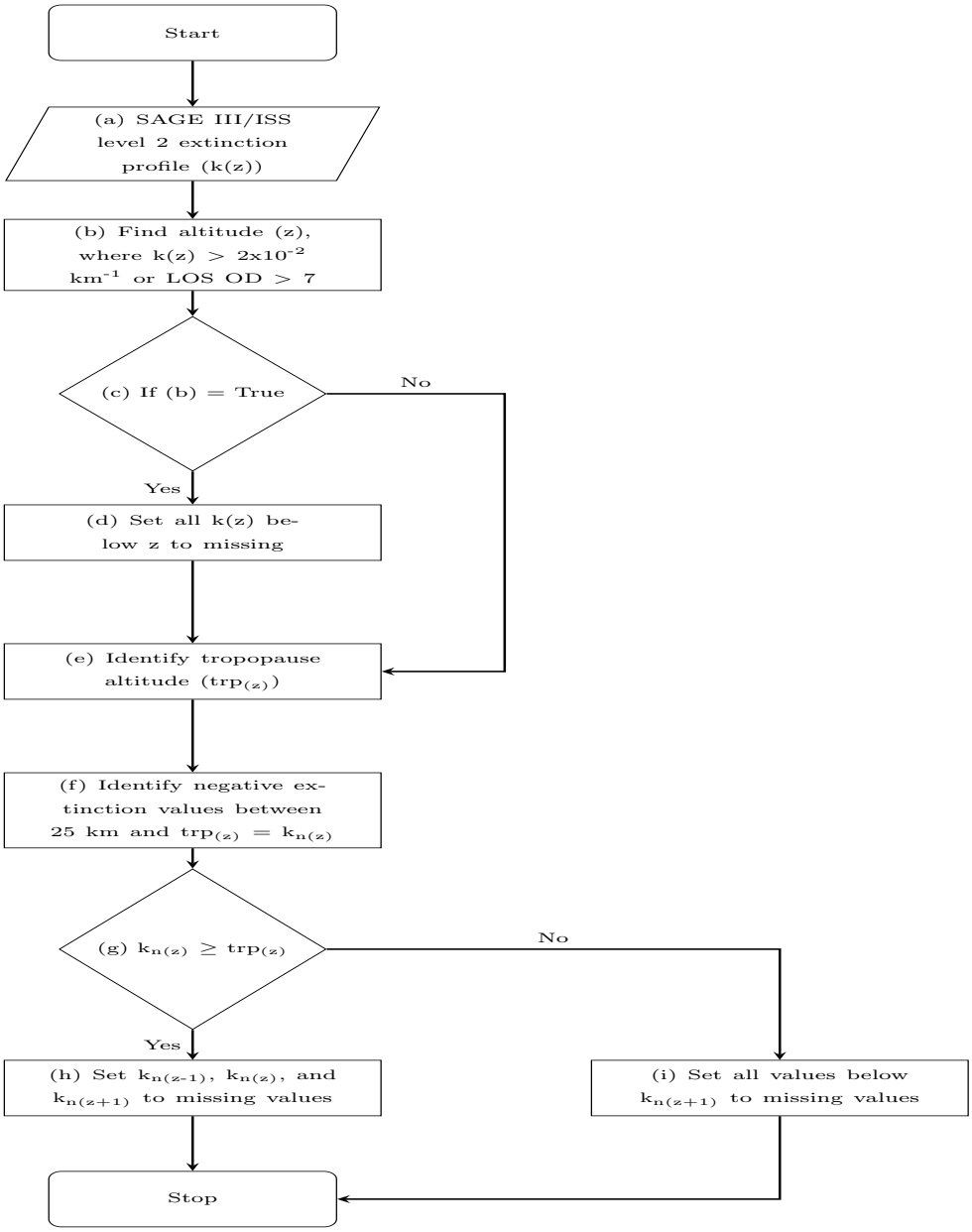

Figure 2. Flow chart of negative extinction coefficient filtering method. $k_{(z)}$ in the flow chart represents extinction coefficient at altitude "z" and (a) through (i) represent steps involved in the filtering algorithm.

3.1 TV13* Method

The TV13* method uses the 525 to 1020-nm extinction ratio to separate between aerosol and aerosol~~extinction efficiency at any wavelength can be computed from Mie theory using the underlying particle size distribution , particle composition through index of refraction, and shape of the distribution. Stratospheric aerosols are primarily sub-micron spherical liquid droplets that are typically composed of sulfuric acid and water (Rosen, 1971)0pt. Particle composition is estimated following Steele and Hamill (1981) 0ptwith index of refraction from Palmer and Williams (1975)0pt. Particle size dependence of extinction efficiency at SAGE III/ISS channels is shown in Figure ??. Further, Figure ??b shows extinction ratios computed from extinction efficiency kernels at~~ cloud mixtures. This is possible because the 525 and 1020 ~~as well as 756~~ nm extinction efficiency kernels ($Q_{(\lambda,r)}$, where Q is extinction efficiency, λ is the wavelength, and r is the radii) and resulting extinction coefficients show significant variations across particle sizes normally observed in the stratosphere. Extinction ratio was computed theoretically from aerosol extinction efficiency using Mie theory (assuming a lognormal distribution and ~~1544 nm that provide information on how extinction ratios are related to particle size. The extinction ratio between 525 and~~ 75% sulfuric acid composition (Rosen, 1971; Steele and Hamill, 1981; Palmer and Williams, 1975)0pt). Figure 3a shows the extinction efficiency for SAGE II and III aerosol channels with the ratios of 521 to 1020 ~~nm becomes unity as particle size approaches~~ and 756 to 1544 nm shown in Figure 3b. The variations with particle radius in Figure 3b show that at larger particle sizes, the dependence on radius becomes invariant so that above a particle size of about 0.5 ~~m, suggesting that it becomes difficult to distinguish aerosol from cloud as the average particle size gets to 0.5 m, which typically occurs following large volcanic eruptions.~~

3.2 ~~TV13 Method~~

~~In this section, we briefly discuss the method employed by TV13, as well as any specific differences between their method and ours. TV13 demonstrated how mutli-wavelength measurements can be used to separate aerosol and aerosol/cloud mixture during the stratospheric background period from 1999 through 2005. The approach used by TV13 was based on the~~ μm, all particles have essentially the same 525:1020 ~~nm aerosol~~ extinction ratio. ~~For their approach, as a first step, a distinction between primary aerosol and enhanced aerosol was made for the data with extinction ratios larger than 2 in order to avoid any possible cloud contamination (smaller extinction ratios with larger extinction coefficients represent larger particles such as clouds). A probability density function of extinction and a median absolute deviation statistic were used to distinguish between the primary aerosol centroid and enhanced aerosol. The separation between primary aerosol and enhanced aerosol (k_0) is computed using median absolute deviation statistics, which is defined as $k_0 = k_a + 3.0$*MAD, where k_a is the median extinction coefficient of the distribution and MAD is the median absolute deviation. TV13 also noted that in the UTLS region, 95% of the data points with extinction ratios greater than 2 lie below the cutoff value k_0. For SAGE measurements, we interpret our data as mixtures of aerosol/cloud because the long path lengths through the atmosphere characteristic of SAGE-like observations see a combination of aerosol and cloud the expected outcome rather than a purely 'cloud' observation. TV13 used an empirical model based on aerosol centroid an artificial cloud centroid with extinction ratio of~~ Under most circumstances, particles of this size, or extinction ratios close to 1~~and an extinction coefficient of 10^{-1} km^{-1}. The aerosol centroid co-ordinates are computed~~

using the median of the distribution. Here, we reproduce this method with specific changes as we compare TV13 method with the new method in the following section.

The TV13 method was modified to facilitate comparison between the results of , are due to the presence of cloud. However, material from intense volcanic eruptions like Mt. Pinatubo or ash, can produce similar ratios (e.g. SPARC, 2006; Legras et al., 2022)0pt. Furthermore, smoke, which often has a roughly grey spectral dependence, can also produce low extinction ratios in the measurements. In TV13method and the new method presented herein (section 2.2). One such change is in the wavelength combination used. While the most commonly used wavelength combinations for SAGE series of measurements are 525 and 1020 nm, we prefer to use a different wavelength combination of 756 and 1544 nm because 756 and 1544 is a wavelength range of a factor of 2, similar to 525 and 1020. Moreover, unlike 525 nm, event termination is less likely to occur at 756 nm channel significantly above 1544 nm channel, particularly when large aerosols/clouds are encountered. Additionally, another reason to select 756:1544 wavelength combination is that the negative bias reported in the 525 nm channel in , this was applied to a period of low extinction levels observed between 1999 and 2005. For our modified TV13* approach, we use SAGE III/ISS (Wang et al., 2020)0pt. TV13 used SAGE II data collected between 1999 and 2005 and broke that dataset up on a seasonal basis. Here, in our analysis we use data collected that include numerous aerosol perturbations. We also use the anomalous negative value process described above in section 3.1. In addition, we divide the SAGE III/ISS data collected between 2017 and 2021. Instead of breaking up the dataset by season, we divide that data according to month and used the 756:1544 nm extinction ratio for the reasons mentioned aboveby month rather than season to facilitate comparisons with the SOATCM (see section 3.3) that will be monthly based due to implementation issues associated with the SAGE III mission.

Figure **??**a depicts the 756 to 1544

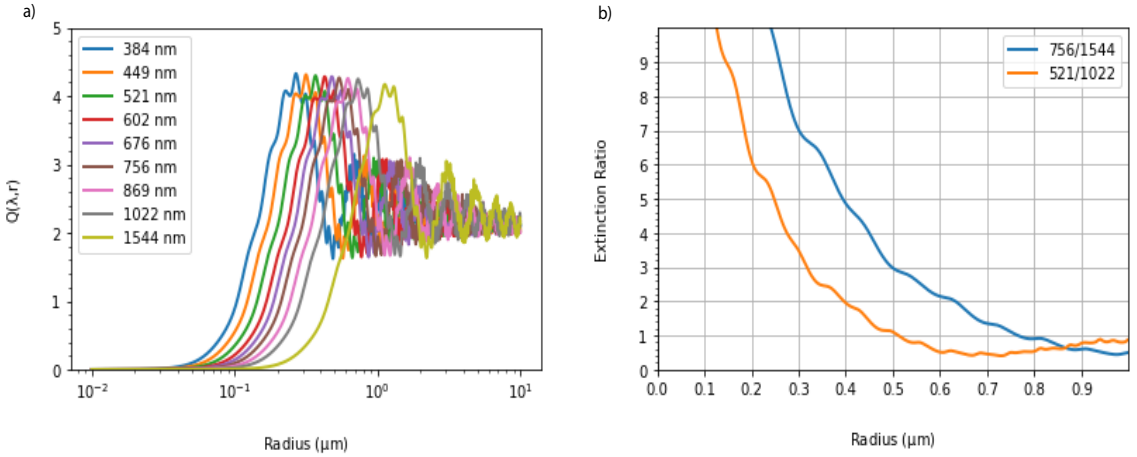

Figure 3. (a) shows Mie extinction efficiency kernel ($Q_{(\lambda,r)}$, where Q is extinction efficiency, λ is the wavelength, and r is the radii) as a function radius for all SAGE III/ISS wavelengths. (b) shows extinction ratios of 521/1022 and 756/1544 computed using extinction kernels from (a) as a function of radii.

Figure 4 shows scatter plot of the 525:1020 nm extinction ratio ($r_{525:1020}$) as a function of ~~1544 nm extinction from SAGE III/ISS measurements~~ 1020 nm extinction for February during the period 2017 through 2021 at an altitude of 15 km~~altitude. The vertical red line in Figure ?? shows k_0, which is computed in the same method as TV13. Here, we reproduce this method using SAGE III data in Figure ??a . Following TV13 method, we use~~ Figure 4 shows a long arm of data that stretch from the aerosol centroid with an extinction ratio of 3.5 and an extinction coefficient of 2.24×10^{-4} toward an extinction ratio of 1 (aerosol centroid is computed using median of the data and is described in detail in the supplementary section S1). While a theoretical $r_{525:1020} = 1.0$ is used to filter out clouds based on Fig. 3b, an offset of 0.4 ~~for the empirical model ratios (R) that accounts for the spread in the aerosol/cloud mixture tail observed in Figure ??a, which is mostly a result of increased measurement noise in 756 nm extinction coefficient. The extinction measurements that are larger than k~~is used, following TV13, to account for the spread we observe in the tail of the scatter plot as extinction ratios approaches unity. We, therefore use $r_{0525:1020}$ ~~but with extinction ratio less than R are considered as aerosol~~$= 1.4$ as the threshold for separating pure aerosol and aerosol/cloud ~~mixtures. It is also noted that there is a wedge-shaped region between k_0 and the modeled curve, which is denoted as "W"~~ mixture. The rationale for using $r_{525:1020} = 1.4$ is further discussed in the supplementary material (section S1).

The TV13* classification process is shown in Figure ~~??. In the~~ 5 and described below:

- We use SAGE III/ISS extinction coefficient data (after screening negative values) as input (Box (a) in Figure 5).
- As a next step toward aerosol and aerosol/cloud mixture classification for the TV13* method, we compute the 525:1020 nm extinction ratios ($r_{525:1020}$) (see Box (b), Figure 5).
- The next step is to compute an absolute deviation based statistic k_{0TV13} (defined as k_a + 3.0*MAD, where k_a is the median extinction coefficient and MAD is the median absolute deviation). This is shown in Figure 5(c) and plotted as a red vertical line in Figure 4 (k_{0TV13} is computed following TV13 by using extinction measurements with $r_{525:1020} > 2$).
- The next step is to isolate extinction coefficients ($k_{(z,\lambda)}$, where k is the extinction coefficient at altitude "z" and wavelength "λ") with $r_{525:1020} > 1.4$ (Box (d), Figure 5).
- We then use $k_{(z,\lambda)}$ and k_{0TV13} to identify perturbed aerosol. If $k_{(z,\lambda)} > k_{0TV13}$ (Figure 5(e)), then $k_{(z,\lambda)}$ is flagged as "Perturbed Aerosol" as shown in Figure 5(f). This is also shown in Figure 4 as data to the right of the red vertical line in the upper right quadrant.
- The next step is to isolate the extinction coefficients $k_{(z,\lambda)}$ with $r_{525:1020} < 1.4$. If $k_{(z,\lambda)} > k_{0TV13}$ with $r_{525:1020} < 1.4$ (Figure 5(g)), then $k_{(z,\lambda)}$ is flagged as "Aerosol Cloud Mixture" as shown in Figure 5(h). This is also shown as data in the lower right quadrant in Figure 4.
- We then use $k_{(z,\lambda)}$ with $r_{525:1020} > 1.4$ to classify standard aerosol. If $k_{(z,\lambda)} < k_{0TV13}$, then $k_{(z,\lambda)}$ is flagged as "Standard Aerosol" as shown in Figure 5(i). This is also shown in Figure 4 as data to the left of the red vertical line in the upper left quadrant.

– The next step is to use extinction coefficient $k_{(z,\lambda)}$ with $r_{525:1020} < 1.4$ to identify standard aerosol. If $k_{(z,\lambda)} < k_{0TV13}$, then $k_{(z,\lambda)}$ is flagged as "Standard Aerosol" as shown in Figure 5(j). This is also shown in Figure 4 as data to the left of the red vertical line in the lower left quadrant.

TV13 ~~method, data that fall in this region were counted as aerosol /cloud mixtures and were removed from further analyses. Figure ??b shows the data after filtering the tail of the distribution and the datathat fall inside the wedge shaped area. The~~ had also used an empirical model based on aerosol centroid, and an artificial cloud centroid with extinction ratio of 1.4 and an extinction coefficient of 10^{-1} km^{-1} to fit the data. A detailed description of the empirical TV13~~method works reasonably well during background periods when there is no enhancement of aerosol so that particle size remains realtively small (< 0.5 m)and there is no ambiguity in the relationship with extinction ratio and the particle size. However , the classification becomes challenging, following volcanic/PyroCb events where the extinction coefficients are enhanced with larger aerosol extinction for which the classification of the tail of the distribution is problematic as shown~~ * model is available in the supplementary section of the paper (section S1).

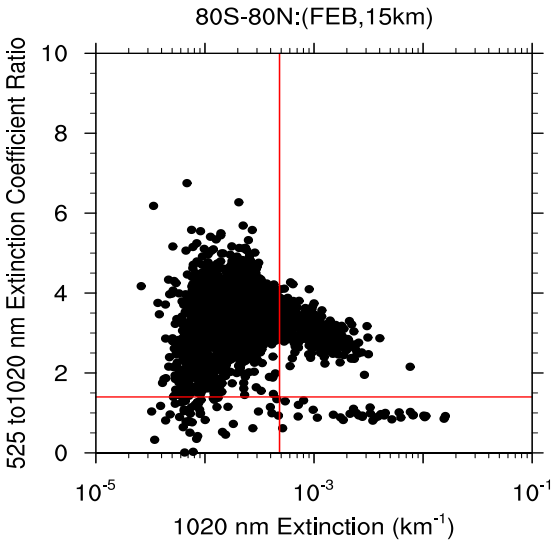

Figure 4. Scatter plot of extinction ratio (525/1020) as a function of 1020 nm extinction coefficient for February at 15 km altitude. Global data between 2017 and 2021 are used for the plot. Vertical and horizontal red lines show k_{0TV13} and $r_{525:1020} = 1.4$ respectively.

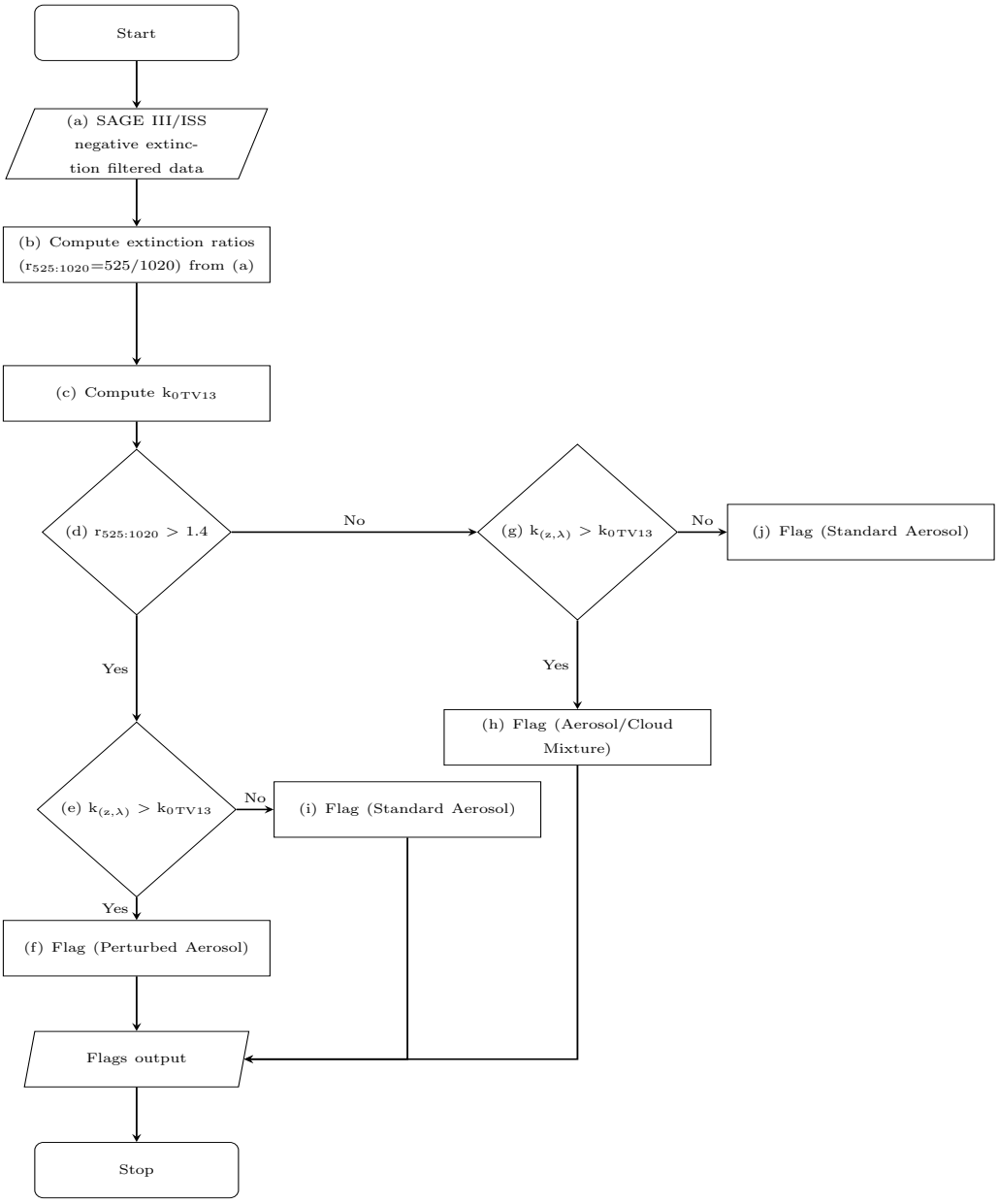

Figure 5. Flow chart of TV13* method. $k_{(z,\lambda)}$ in the flow chart represents extinction coefficient at altitude "z" and wavelength "λ", whereas $k_{0TV13} = k_a + 3.0$*MAD. k_{0TV13} is computed following TV13 by using extinction measurements with $r_{525:1020} > 2$. It should be noted that the steps involved ((b) through (j)) in the flowchart is same as TV13 method, except that the seasonal data between 1999-2005 were used for the method presented in TV13. For our analyses, instead of seasonal data, we use monthly data collected between 2017 and 2021.

3.2 Perturbed Stratosphere and SOATCM.

SOATCM is similar to the TV13* method above. However there are several changes which are outlined below and summarized in Figure ??. In such cases, the enhanced aerosol could be mixed with aerosol/cloud mixture category as they are likely filtered out from the aerosol category, which could potentially result in an underestimation of aerosol extinction coefficient . Such cases can frequently occur in the vicinity of the tropopause or in the lower stratosphere where many such enhanced aerosols could be mis-classified as aerosol/cloud mixtures. We also note that perturbed events can cause more than one aerosol centroid which is due to inter-hemispheric differences in the data following the events. In Figure ??, there appears to be two clusters in the background aerosol region, which is a result of perturbed events. In the following section, a modified approached of 7. The first change is the aerosol extinction coefficient wavelengths used in the process. While the approach used by TV13with classifications is described.

3.3 Perturbed Stratosphere and New Method.

For * method was based on the 525:1020 nm extinction ratio, we used the 756: 1544 nm extinction ratio for the SOATCM. The rationale for using the 756:1544 nm wavelength combination is threefold: 1) the SAGE III/ISS aerosol extinction, we have an advantage of additional wavelength measurements including a longer wavelength (1544 nm) that can be used for the analyses. As noted above, while SAGE III/ISS measurements have been used in many studies, due to a reported negative bias in the 521 nm aerosol extinction measurement is subject to known artifacts, 2) the 756 and 1544 nm wavelength pair are about a factor of two different (comparable to the 525nm channel (Wang et al., 2020)0pt, we now apply a simple correction by spectrally interpolating extinction between 450 :1020 nm ratio used in TV13 for SAGE II), and 3) unlike the 525:1020 nm extinction ratio, 756nm channel using Ångström exponent (Knepp et al., 2021)0pt. While the most commonly used wavelength combinations for SAGE series of measurements are 525 and 1020 nm, due to the reasons listed in section 2.1, we prefer to use a different wavelength combination of :1544 nm extinction ratio extends particle size differentiation to large sizes. Fig. 3b shows the theoretical 756and 1544. We, however compared :1544 ratio as a function of particle size and demonstrates that the ratio retained sensitivity to particle size changes up to ≈0.8 μm rather than 0.5 μm for the 525and :1020 nm wavelength combination for historical reasons and observe that both wavelength combinations (ratio. Therefore, the 756/:1544 wavelength combination allows size discrimination at lower altitudes in the lower troposphere where larger aerosol particles can be observed following volcanic eruptions (e.g., ash) and we used the 756:1544 nm and 525 /1020 nm) yield similar results in the stratosphere (not shown here)extinction ratio for the SOATCM proposed here.

SAGE III/ISS data witnessed many small to has borne witness to a number of moderate eruptions and several PyroCb events that reached the stratosphere . (see Table 1lists those events with event date and latitude of occurrence. The frequency of occurrence of these events make it more). Given the frequency of events that enhance the aerosol extinction, it is challenging to employ a cloud screening algorithm for SAGE III/ISS . An enhancement of aerosol extinction following these events is therefore important as in some cases, enhanced aerosols could be large enough to be misinterpreted as clouds, particularly when they are mixed with aerosol/cloud mixture in the tail of the distribution shown in Figure ??a . Our goal here is to first

identify enhancement in aerosol extinction following these events and the time it takes to get back to the background level. We, therefore analyzed the data following these events to look for enhanced aerosol loading. We then employed an approach to look for any enhancement in the data based on median absolute deviation statistics to compute outliers in the data. The outliers for these events are in fact perturbed extinction coefficients. based solely on the presence of outliers without a substantial risk of denoting volcanic or smoke-related enhancements as 'cloud'. In developing SOATCM, we found it critical to identify instances of enhanced aerosol within the observations and track that enhancement as it dissipates. Median absolute deviation statistics is are computed on a monthly basis with a 20 degree latitude band that is centered at the volcanic/fire event latitude. We, then define an outlier extinction coefficient from the monthly probability density function distribution. The Following Iglewicz and Hoaglin (1993)0pt, we define an outlier extinction coefficient, k_0= , as k_a + 3.5*MAD, where k_a is the median extinction coefficient of the distribution and MAD is the median absolute deviation. We use a factor of 3.5 to estimate outlier based on modified Z-scores of a simulation study (Iglewicz and Hoaglin, 1993) 0ptthat shows an absolute value of 3.5 can be used to define potential outliers in the above equation.

Figure ?? Figure 6 shows a time series of k_0 for 1544 nm for various latitude bands for all events shown in Table 1. 1 with points we consider 'enhanced' denoted in red. Based on the k_0 time series, the timeframe time frame of volcanic/fire event is determined. k_0 is an estimate of the extreme value that represents the enhancement of extinction coefficient due to any volcanic/fire event. For each event, the we track the enhancement in aerosol extinction following an event and the time it takes to get back to the background level using the red symbol shown in the time series plot. The altitudes are chosen in such a way that they represent average tropopause altitude for each latitude band. In the vicinity of tropopause, separating aerosols from clouds is always challenging, particularly following such events as it becomes hard to distinguish between background as well as enhanced aerosol/clouds (Thomason and Vernier, 2013)0pt. We therefore make use of the timeframe from the time series plots that will be incorporated in the cloud algorithm so that we are able to track the event and retain the data in the vicinity of the tropopause with a different flag named " Volcanic Aerosol/Tropopause Cloud". A detailed description of flags in the data will be discussed in Section 2.2.2. The computation of time series step is shown as box (b) in the flowchart (Figure 7).

3.2.1 Identifying centroid of the distribution based on measurements.

The first step in the cloud-screening was to estimate the influence of perturbed events based on the time series plot for different latitude bands. While we follow the

Table 1. Volcanic and PyroCb events used in this study

Event Name	Event Date	Latitude
Canadian Wildfire (Cw)	17 July 2017	51N
Ambae Eruption (Am)	28 July 2018	15S
Ulawun Eruption (Ul)	22 June 2019	5S
Raikoke Eruption (Ra)	03 August 2019	48N
Australian Wildfire (Aw)	31 December 2019	34S
California Creek Fire (Cc)	01 September 2020	37N
La Soufriere (La)	22 April 2021	13N
McKay Creek Fire (Mc)	29 June 2021	54N

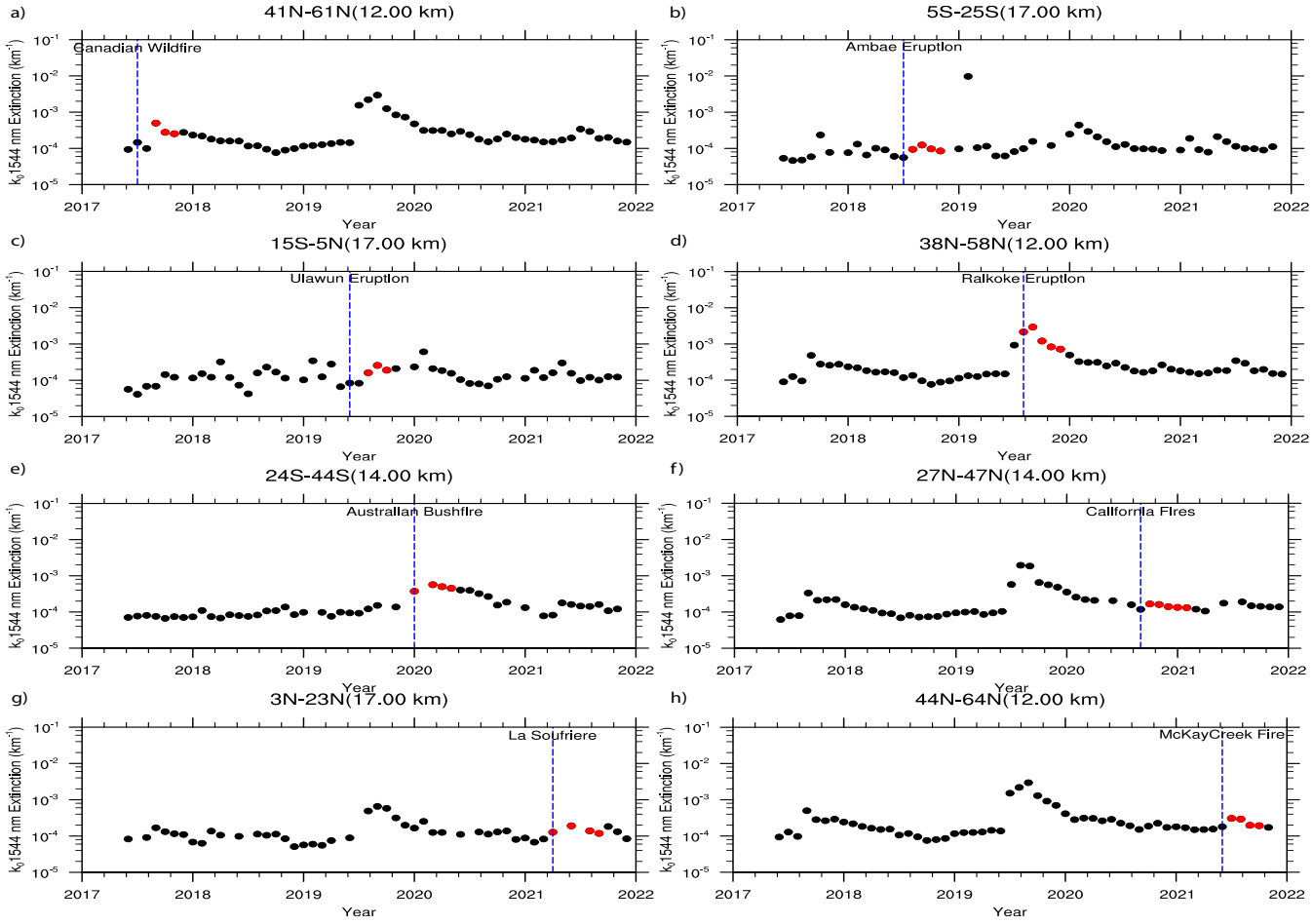

Figure 6. Time series of k_0 1544 nm extinction for different latitude bands. Red symbols show the time line of enhanced aerosol extinction coefficient and the time it takes to get back to the standard aerosol level following each event. The panels show events listed in Table 1 with (a) Canadian Wildfire, (b) Ambae eruption, (c) Ulawun Eruption, (d) Raikoke Eruption, (e) Australian Wildfire, (f) California Creek Fire, (g) La Soufriere and (h) McKay Creek Fire. The altitudes shown in figure are the averaged tropopause altitude for the respective latitude band.

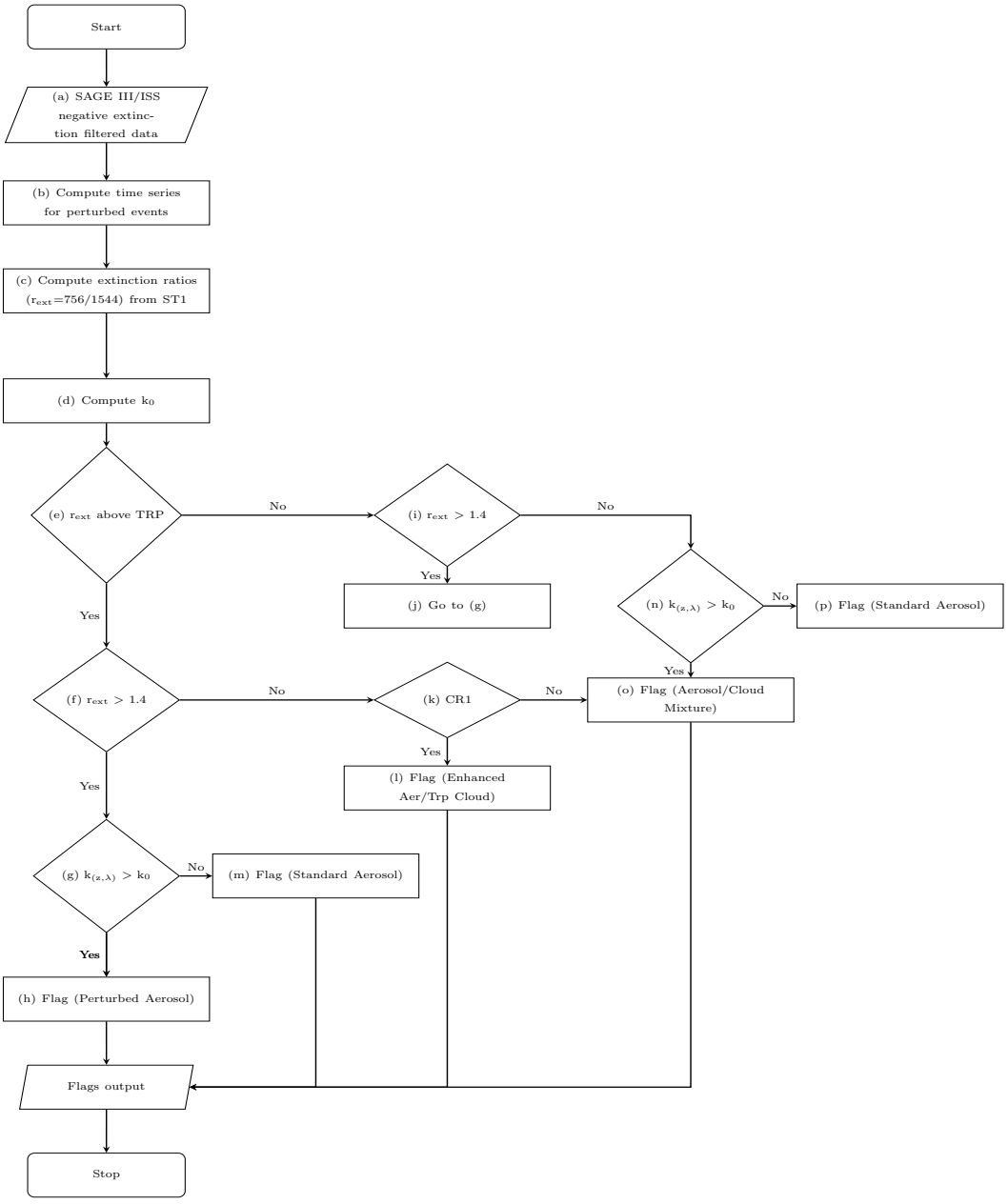

Figure 7. Flow chart of the SAGE III Operational Aerosol Type Classification Method. $k_{(z,\lambda)}$ in the flow chart represents extinction coefficient at altitude "z" and wavelength "λ", whereas $k_0 = k_a + 3.5$*MAD. TRP in the flowchart represents tropopause altitude and (a) through (p) represent steps involved in the algorithm. The influence of the perturbed event on extinction is decided on whether an extinction coefficient data point falls within the prescribed latitude band which is based on a perturbed event (Figure 6) and whether the extinction ratio falls below 1.4. This is shown as CR1 in the flowchart.

Another difference between TV13~~method, some modification to their work is needed in order to incorporate influence of volcanic/fire events. So, the next step is to locate the aerosol centroid from the extinction ratio versus extinction plot so that we could effectively implement the aerosol model used in~~ * and the SOATCM, is that statistics for TV13* are accumulated based on the global data set.

~~For the TV13 method, we used median of the distribution of the global data on a monthly basis.~~ However, for SAGE III/ISS, we noticed that the perturbed events cause inter-hemispheric differences in the data, leading to more than one cluster in the data. Figure ~~??~~ 8 shows scatter plots of extinction ratio versus extinction for two of the perturbed events. The upper panel of the figure shows how extinction ratios (756/1544) change with respect to 1544 nm extinction, following the Canadian Wildfire event ($\sim 51^0$N) that occurred in August ~~2017.~~ 2017, whereas the lower panel shows the same but for the Ambae eruption ($\sim 15^0$S) in July 2018. While all of the data are plotted, we use different colors for different latitude bands to show the influence of any such event in the data. ~~Please note that the~~ The data presented in Figure ~~??~~ 8 was plotted at 2 altitudes: 11 km (panels a-d) and 17 km (panels e-h). The 11 km altitude was ~~used~~ chosen because it is approximately representative of the average tropopause height for this latitude band and the 17 km altitude is chosen because it represents approximate tropopause altitude for the tropics. It is evident from the figure (panels a-d) that there is a distinct enhancement of extinction coefficient in the northern latitude band (20°N-80°N) following the ~~event while outlier statistics show that the data points fall beyond the k_0 value are clearly enhanced extinction from the perturbed event~~Canadian Wildfire event (Figure 8 b-d). Similarly, the lower panel shows data following the Ambae eruption in July 2018 and demonstrates distinctly enhanced extinction (Figure 8 f-h) from the southern latitude band (80°S-20°S). Additionally, these global monthly data plots suggest there are inter-hemispheric differences in extinction ~~coefficient.~~

~~Locating the aerosol centroid is challenging, particularly following a volcanic/fire event as it is evident from Figure ?? that there are more than one cluster with inter-hemispheric differences.~~ ratios. Therefore, we ~~employed an unsupervised machine learning clustering algorithm called as "k-medoid clustering" (e.g. Kaufman and Rousseeuw, 1990; Park and Jun, 2009)0pt. The K-medoid clustering algorithm is more robust in identifying noise and outliers as it picks one of the cluster members as the medoid (a medoid is a data point that has the shortest total distance to other members of the cluster). For the analyses here, we use two medoids that are based on the scatter plots shown in Figure ?? . We tested our algorithm on the global data and it works reasonably well in identifying the centroid in the extinction ratio plots shown in Figure ?? . While the algorithm works well in most cases, with the inter-hemispheric differences that we see in the data, we decided to implement the clustering algorithm for different latitude bands to avoid any bias in identifying centroids. We, therefore~~ divided monthly data into two latitude bands: 1) 80°S-20°N, and 2) 20°N-80°N. Initially, the tropical latitude band (20°S-20°N) was used as a separate ~~latitude band but lack~~ band but paucity of tropical data for statistical analysis forced us to combine the tropical latitude band to the southern latitude band (80°S-20°S). ~~We, therefore~~ Therefore, we perform aerosol categorization based on these two latitude bands (80°S-20°N and 20°N-80°N), which will be described in the following section.

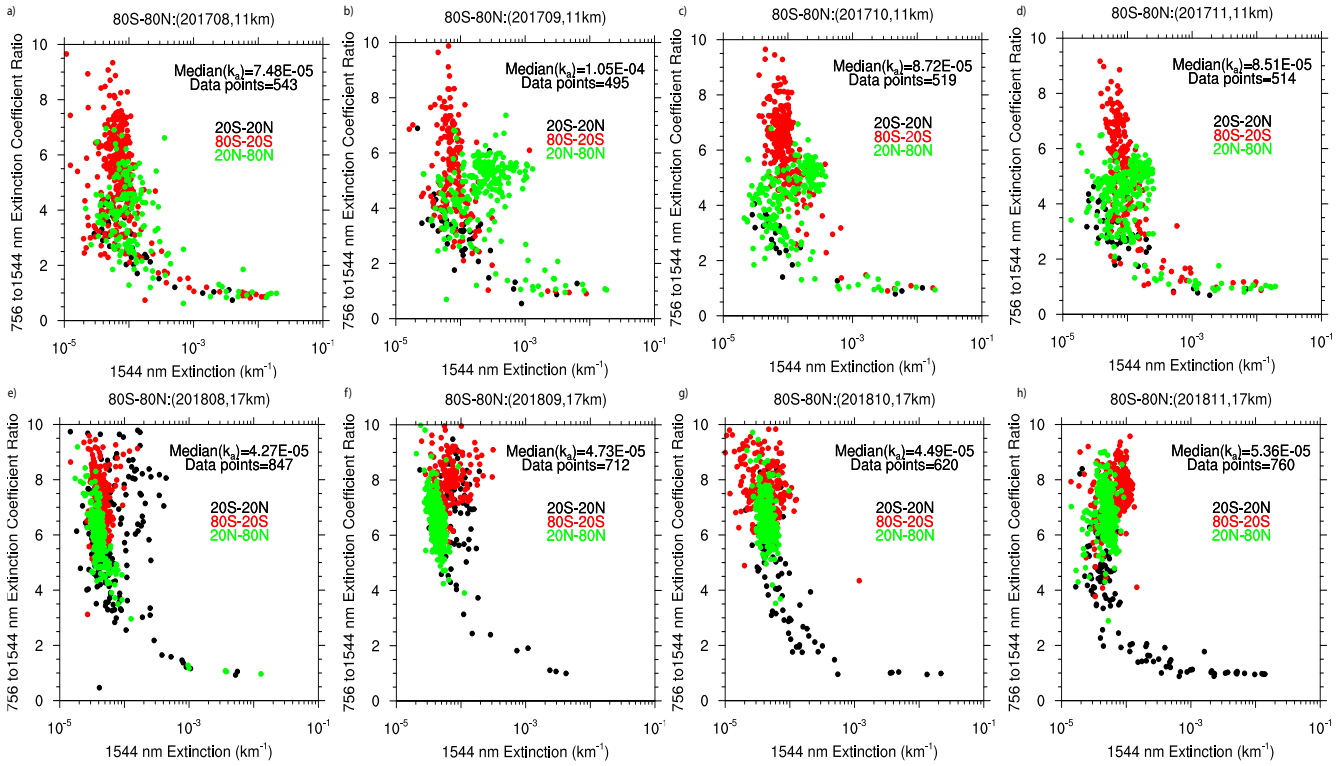

Figure 8. Scatter plots of 756 to 1544 nm extinction ratio versus 1544 nm extinction following the Canadian Wildfire event in 201708 (a-d) and the Ambae eruption in 201807 (e-h). The upper panel shows scatter plots of extinction ratio versus extinction at 1544 nm for August 2017 through November 2017 for an altitude of 11 km (a-d), whereas the lower panel shows the same but for August 2018 through November 2018 at 17 km.

3.2.1 Categorizing aerosols and aerosols-cloud mixtures

~~While we follow the method used in TV13, a modified approach is used here as SAGE III~~

Figure 7 shows the flowchart for the SOATCM. The steps involved in categorizing aerosols/~~ISS data record has several low to moderate volcanic eruptions and some extreme fire events which makes separation of aerosol from aerosol-cloud mixtures challenging. In Figure ?? , we show how aerosol/categorization is done by showing examples of two perturbed events: (a) Canadian Wildfire and (b) Ambae eruption that occurred at 51N and and 15S respectively. In our revised method , we use monthly median absolute statistics to estimate the outlier extinction coefficient (k_0) . The vertical red solid line in each plot represents k_0, whereas the horizontal red lines indicate the location of a hypothetical~~ clouds using SOATCM is described below:

- We use the SAGE III/ISS extinction coefficient data (after screening negative values) as input (Figure 7(a)).
- The next step is to compute the time series (Figure 6) to determine the influence of any perturbed event (Figure 7(b)).

- We then compute the extinction ratios between 756 and 1544 nm (Figure 7(c)).

- The next step is to compute monthly median absolute statistics (k_0) to estimate the outlier extinction coefficient. This is shown as Figure 7(d) and as a vertical solid line in Figure 9. It should be noted that k_0 is computed at each altitude.

- We then used r_{ext} and the tropopause height (TRP in Figure 7) to separate data below and above tropopause (Figure 7(e)).

- An extinction ratio (r_{ext}) of 1.4 is then used as the threshold for separating aerosol and aerosol/cloud mixture due to the reasons mentioned above in the TV13* method (While clouds nominally are expected to produce ratios of close to 1 in these measurements, many cloud observations are mixtures of aerosol and clouds thus ratios greater than 1 for observations that are inferred as cloud are common. The value of 1.4 is based on observations of the behavior of both SAGE II and SAGE III data sets.). Data is treated differently whether it is above or below the tropopause. As a next step, we use data above the TRP and use extinction coefficients with $r_{ext} > 1.4$ (Figure 7(f)).

- If $r_{ext} > 1.4$ and extinction coefficient ($k_{(z,\lambda)}$, where "z" is the altitude and λ is the wavelength) is greater than k_0 (Figure 7(g)), then $k_{(z,\lambda)}$ is flagged as "Perturbed aerosol" (Figure 7(h)). Figure 9 shows how the aerosol/cloud categorization is done by showing examples of two perturbed events: (a) the 2017 Canadian Wildfire and (b) the 2018 Ambae eruption that occurred at $\sim 51°$N and $\sim 15°$S respectively. The "Perturbed aerosols" are shown as pink filled circles in Figure 9. The vertical red line in Figure 9 represents k_0.

- We then look at the data below the tropopause and check if $r_{ext} > 1.4$. If $r_{ext} > 1.4$ is "true", then the data are treated as stratospheric and the algorithm goes to step (g) as shown in Figure 7(j).

- If $r_{ext} < 1.4$ and the data are above the TRP, then we use a different criterion (CR1). CR1 in Figure 7(k) is dependent on the time series results from Figure 6. We use enhanced extinction values (red filled circles) shown in Figure 6 for each event and for latitude band within 20°of the latitude of occurrence of any perturbed event. The influence of the perturbed event on extinction is decided based on whether an extinction coefficient data point falls within the prescribed latitude band which is based on a perturbed event and whether the extinction ratio falls below 1.4 based on Figure 6. If the data fall within the time frame and latitude band of perturbed event based on time series analysis (CR1 = True in Figure 7), then we flag them as "Enhanced Aerosols/Tropopause Cloud" (Figure 7(l)). These data points are shown as orange filled circles in Figure 9. While these large particles (≥ 0.8 μm) with $r_{ext} < 1.4$ and under background conditions are identified as "aerosol/cloud mixture", which may not be true under perturbed conditions (Figure 9) where larger particles could be from the perturbed event that are actually enhanced aerosols, which could be misidentified as "aerosol/cloud mixture". While we use the time frame and latitude band of the perturbed event based on Figure 6, a caveat on the "enhanced aerosols/tropopause cloud" flag is that these enhanced aerosols could be mixed with clouds or could just be clouds, particularly in the vicinity of the tropopause. We, therefore use "enhanced aerosols/tropopause cloud" rather than just "enhanced aerosols" so that the possibility of cloud is not completely overruled, particularly when the data fall in the region just above the tropopause.

- If $r_{ext} > 1.4$ and the data are above the TRP with $k_{(z,\lambda)} < k_0$, the algorithm flags those data points as "Standard aerosol" as shown in Figure 7(m). These data points can also be seen in Figure 9 as green filled circles.

- If $r_{ext} < 1.4$ and the data are below the TRP, then the algorithm checks if the extinction coefficient $k_{(z,\lambda)}$ is greater than k_0 as shown in Figure 7(n). If $k_{(z,\lambda)} > k_0$, then $k_{(z,\lambda)}$ is flagged as "Aerosol/Cloud mixture" (Figure 7(o)). This can also be seen in Figure 9 as blue filled circles.

- Finally, if $r_{ext} < 1.4$ and extinction coefficient $k_{(z,\lambda)}$ (below the TRP) is less than k_0, then $k_{(z,\lambda)}$ is flagged as "Standard aerosols" (Figure 7(p)). This can also be seen in Figure 9 as green filled circles.

Additionally, we used an empirical model to fit the observed data, following TV13* method, which is also discussed in detail in section S2 of the supplementary material.

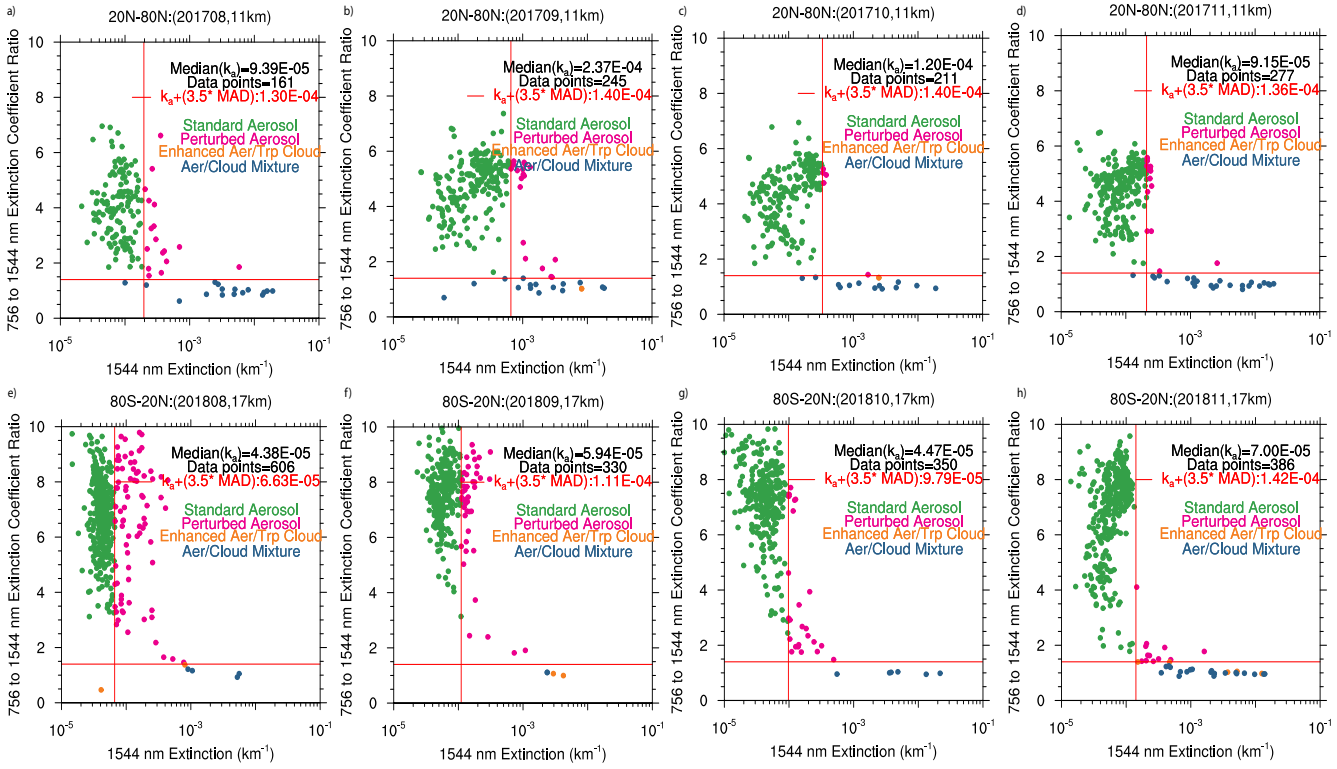

Figure 9. Scatter plots of the 756 to 1544 nm extinction ratio versus 1544 nm extinction following the Canadian Wildfire event in 201708 (a-d) and the Ambae eruption in 201807 (e-h). The upper panels show scatter plots of extinction ratio versus extinction at 1544 nm with aerosol/cloud categorization for August 2017 through November 2017 for an altitude of 11 km (a-d), whereas the lower panels show the same but for August 2018 through November 2018 at 17 km.

3.3 Comparison between TV13* and SOATCM

Due to the limitations of the wavelength combinations (525:1020 nm) used in the TV13* method as outlined in section 3.1 , there is a possibility that some of the larger aerosols ($> 0.5\ \mu$m) in the TV13* method could be classified as aerosol/cloud mixture~~'s extinction ratio of 1 with a fixed offset of 0.4 similar to TV13. We therefore divide the plotting area into four quadrants based on k_0 and an extinction ratio of 1.4. The upper left quadrant is identified as~~ , particularly following a perturbed event. For the comparison between TV13* and the SOATCM, we show profiles of extinction coefficient at 1544 nm following two perturbed events. Figure 10 shows extinction coefficient profile plots at 1544 nm for two cases following the Canadian Wildfire (upper panel) event and the Ambae eruption (lower panel) respectively.

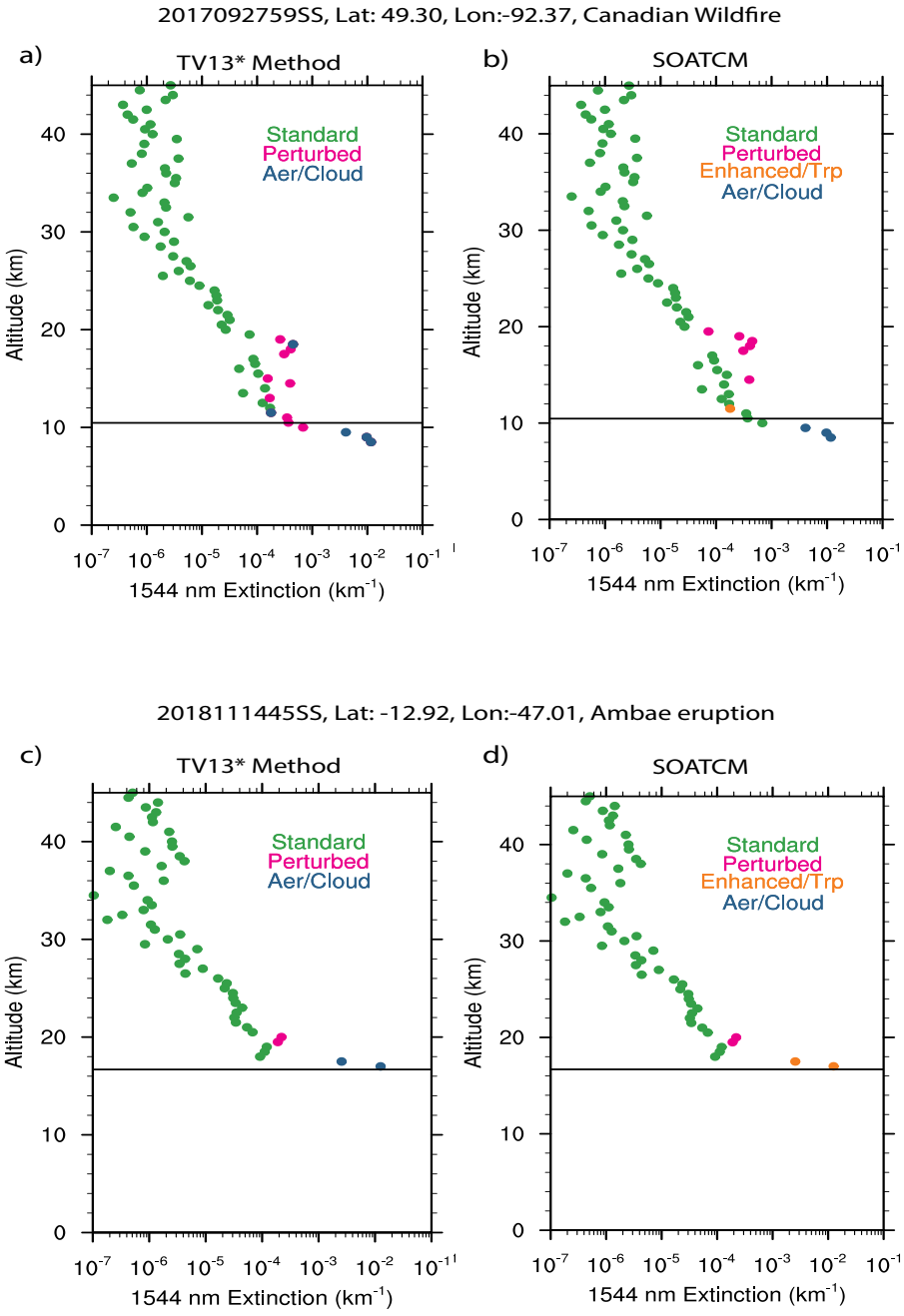

Figure 10. Aerosol/Cloud categorization of extinction profiles at 1544 nm for the Canadian Wildfire and the Ambae eruption. The upper panels show extinction profile comparison between the TV13* method (a) and SOATCM (b), following the Canadian Wildfire, while the lower panel shows the same comparison but for a profile, following the Ambae eruption. The event date for the profile for (a,b) is 27 September 2017 (Latitude: 49.30° and Longitude: -92.37°) and for (c,d) is 14 November 2018 (Latitude: -12.92° and Longitude: -47.01°).

While there are some similarities between the two methods in categorizing "backgroundstandard" aerosol, while data in the upper right quadrant represent and "perturbed" aerosol. However, the data points that fall in the lower two quadrants are difficult to categorize. Since the extinction ratio is less than 1.4 and extinction value greater than k_0 then those particles are large enough to be misinterpreted as clouds, following a volcanic/fire event . We, therefore implemented a different method that dictates how flags are determined in the lower two quadrants. We use time frame from the time series analysis shown in Figure **??** for each event and for latitude band within 20of the latitude of occurrence of any perturbed event. The influence of the perturbed event on extinction is decided on whether an extinction coefficient data point falls within the prescribed latitude band which is based on a perturbed event and whether the extinction ratio falls below 1.4. While, aerosols, there are differences that arise from the differing statistical methods and the differing wavelength combinations used in each method. While TV13categorized this lower tail of the distribution as * method works reasonably well in categorizing standard and perturbed aerosols based on long term monthly statistics (all data collected between 2017 and 2021 for each month), the SOATCM uses month to month data to compute statistics and therefore is a better representation of categorization based on monthly statistics.

The important difference between TV13* and the SOATCM method is in categorization of "aerosolenhanced aerosols/cloud mixturetropopause cloud", we make use of time and latitude of the event along with tropopause height to incorporate the . For the SOATCM, we use the influence of any perturbed event . Based on the time frame (the red symbols based on a time series as shown in Figure **??**) after each event, we additionally use a tropopause height data as the lower altitude range for which this method is valid. For the circumstances 6 and use $r_{ext} \leq 1.4$ and $k_{(z,\lambda)} > k_0$ to identify "enhanced aerosols/tropopause cloud". This categorization is made only above the tropopause altitude where enhanced extinction coefficient with $r_{ext} \leq 1.4$ could occur as a result of a perturbed event. However, there could be a possibility of confusing with aerosols and clouds or just clouds at these altitudes. We do apply this category only when the above mentioned criteria is met in the stratosphere. As a result, we then relax the "Aerosol/Cloud Mixture" category and flag them as "Enhanced aerosol/Tropopause cloud" based on the above criteria, whereas the data that do not fit the above criteria is flagged as "Aerosol/Cloud Mixture". By doing this, we retain some of the near tropopause data that may have been influenced by such perturbed events that were otherwise classified these data points as "aerosolenhanced aerosols/cloud mixture" in TV13 method. The "enhanced aerosol/tropopause cloud"flag is now added to the aerosol category for all our analyses. The viewing geometry of SAGE III/ISS is such that separating enhanced aerosols from clouds in the vicinity of UTLS is otherwise difficult.

Figure **??** represents the revised aerosol/cloud categorization. The upper panel in Figure **??** shows scatter plots of 756/1544 extinction ratio versus 1544 extinction for 20N-80N following . This can be seen in Figure 10 b, for a profile that is influenced by the Canadian Wildfire event in 2017. It is clearly evident that an enhancement in extinction coefficient occurs following the event particularly in the 20N-80N latitude band with aerosol centroid coordinates clearly suggesting an increase in 1544 nm extinction and a decrease in the extinction ratio. We use different flags to identify different types of aerosolsas mentioned above. The plots shown in Figure **??** are for an altitude of 11 km and the "enhanced aerosols/tropopause cloud" categorization is made at 11.5 km (orange filled circle), whereas Figure 10 d shows the same but for the Ambae eruption at 17 km , which is roughly the tropopause altitude for the latitudes where Canadian Wildfires and Ambae eruption occurred. So, with the criteria used above, we classify the near tropopause aerosol following any event within a latitude band of 20 degree centered

at the event latitude & 17.5 km. It is to be noted that for these two cases, the TV13* method flagged these data points as "Enhanced Aerosolaerosol/Tropopause Cloudcloud mixture" (Green symbols in Figure ??). The Figure 10 a&c). Therefore, the important difference between TV13* method and the SOATCM is the way "Enhanced Aerosolenhanced aerosols/Tropopause Cloudtropopause cloud" flag is added into the aerosol category in all the analyses. This may cause an enhancement in aerosol extinction coefficient but we retain these data points because they might contain important information on enhanced aerosols from the perturbed event. An empirical model is fit to the observations following Equation 4 of is treated. Additionally, for the TV13, which is shown in Figure ??. The model is computed using information on aerosol and cloud centroid co-ordinates. TV13 use median of the distribution to locate aerosol centroid whereas the current method used * method extinction ratio of 525:1020 nm ($r_{525:1020}$) was used and therefore it is possible that larger particles with radii roughly > 0.5 μm could be flagged as "k-medoid clustering" described in section 2.2.2 to locate aerosol centroid. The cloud centroid co-ordinates are empirically determined as 1544 nm extinction and 756 to 1544 nm extinction ratio being set to $1.0X10^{-1}$ km $^{-1}$ and 1.4 respectively, similar to TV13 method.

3.4 Comparison between TV13 and New Method

We compare TV13 method and the new method after filtering out possible aerosol/cloud mixture" (based on Figure 3b). Figure ?? shows scatter plot of 756 to 1544 nm extinction ratios as a function of 1544 nm extinction at two different altitudes. The data shown in Figure ?? is for the period 2017-2021 for their respective altitudes. Figure ?? depicts the entire SAGE III10a shows one such cases at 18 km, where the data is flagged as "aerosol/ISS data at 11 and 17 km. The noted difference in the new method is that the retention of some of the data in the tail of the distribution between extinction ratio of 1.4 and 2.0, whereas cloud mixture", whereas Figure 10b flag that data point as perturbed aerosol. We provide several other cases of comparison between TV13method removes the data in this region as it is evident in Figure ??a, c. TV13 method, however retains data that fall in the lower left quadrant where extinction ratios are less than 2.0 and for extinction less than k_0, whereas in the new method these data have been removed as these data with smaller extinction ratios and relatively smaller extinction coefficients are possibly of larger extinction uncertainty and are less reliable. For * and the SOATCM in the supplementary section (section S3), which shows similar results. Eventually, the latitudes > 55, SOATCM method will be used to produce a level 3 SAGE III/ISS aerosol product.

For the SOATCM, in addition to the listed categorization, we make an effort to identify polar stratospheric clouds (PSC) in the new method by applying for the latitudes $> 55°$ using a temperature based filter. The PSCs are filtered out when the ambient temperature falls below 200K (not shown here).

4 ~~Implications of cloud-screening on GloSSAC~~

3.1 Application of the SOATCM to the Global Space-based Stratospheric Aerosol Aerosol Climatology (GloSSAC)

Stratospheric aerosol is an important component in determining the radiative and chemical balance of the atmosphere. Many Global Climate Models (GCMs) do not have an interactive aerosol module to treat stratospheric aerosol and therefore depend on global measurements on a long-term basis. Therefore, the Global Space-based Stratospheric Aerosol Climatology (GloSSAC) was created first in 2018 (Thomason et al., 2018) to support the climate modeling community for ~~Couple~~ the Coupled Model Intercomparison Project Phase 6 (CMIP6) project (Eyring et al., 2016). For GloSSAC, the SAGE series of measurements play a vital role in the long-term data starting from 1979 through present, excluding post-SAGE II era (August 2005-May 2017) during which other space-based measurements were used to fill the gap (e.g. Thomason et al., 2018; Kovilakam et al., 2020). ~~While other measurements were available to fill the gap for the post-SAGE II era, an~~ An important factor missing in those measurements ~~were~~ was measurements of extinction coefficient at multiple wavelengths. For GloSSAC version 2.0 (Kovilakam et al., 2020), we extended the data set to December 2018 with the inclusion of the SAGE III/ISS multiple wavelength data from June 2017. ~~It is known that the presence of cloud in the vicinity of the UTLS makes it challenging for SAGE measurements to identify and separate pure aerosol from aerosol cloud mixture/enhanced aerosols, particularly following a perturbed event such as volcanic eruption or PyroCb as removing those data points (i.e. lower extinction ratios with higher extinction coefficients) could lead to an underestimation of aerosol extinction in the UTLS region.~~ Recent changes in the stratospheric aerosol loading in the UTLS region have received significant attention in the scientific community (e.g. Bourassa et al., 2012; Vernier et al., 2015) as increased aerosol loading in this region can have larger impact on radiative and chemical balance. Therefore, it is important to identify aerosols more accurately in the vicinity of the tropopause particularly following events that perturb the stratosphere.

For GloSSAC version 2.0 (v 2.0) (data product released in 2020 with data extended until 2018 (Kovilakam et al., 2020)0pt), SAGE III/ISS aerosol extinction coefficient data has been incorporated with a simple extinction ratio based cloud filter approach (data with extinction ratio (525/1020 nm) $>$ 2.0 are only used as aerosols) to avoid any possible cloud contamination in the aerosol extinction data. By using this simple method, some enhanced aerosols from any perturbed event (e.g. volcanic eruptions, PyroCb events) may have been mistakenly flagged as clouds during SAGE III/ISS measurements, particularly in the vicinity of the tropopause and lower stratosphere. It is therefore important to address this issue in the aerosol data, particularly when it is used for a long-term climatology such as GloSSAC. Therefore, we incorporate the revised cloud screening method described in section ~~2.0 into the~~ 3.2 into the latest GloSSAC version 2.2 (v 2.2).

~~Here, SAGE III/ISS data is zonally averaged into 5latitude bins, and 0.5 km altitude resolution on a monthly basis and incorporated into GloSSAC . Additionally, for this version (v2.2), we perform a linear interpolation along time axis to fill in missing values at higher latitudes. For a future release, we plan to implement a reconstruction method for SAGE III/ISS to fill in missing data— a method similar to the one used for SAGE II in GloSSAC version 1.0 (Thomason et al., 2018)0pt. It should also be noted that we now use version 5.2 SAGE III/ISS products in GloSSAC (v2.2) with revised cloud screening algorithm, whereas SAGE III/ISS version 5.1 was used in GloSSAC (v2.0) (Kovilakam et al., 2020)0pt. Figure ?? shows the~~

impact of revised cloud screening algorithm on SAGE III/ISS aerosol data. For the cloud screened product, we use three flags from the cloud screen algorithm, which are "Standard aerosol", "Perturbed aerosol", and "Enhanced Aerosol/Tropopause Cloud" respectively. We also note that the usage of "Enhanced Aerosol/Tropopause Cloud" flag as aerosol in the cloud screened product may introduce a positive bias in aerosol extinction, particularly in the vicinity of tropopause where separating aerosol from aerosol/cloud mixture is challenging. However, by using the timeframe shown in the monthly time series of k_0 in Figure **??** could alleviate the bias to some extent. Figure **??**a,b shows zonally averaged altitude versus latitude plots of extinction coefficients at 525 nm for version 5.1 and 5.2 respectively. The impact of cloud screening is evident from Figure **??**b with a clear enhancement in extinction coefficient in the latitudes $>$ 40N, particularly in the lower stratosphere. The enhanced extinction in version 5.2 is further evident from Figure **??**c, which shows the ratio of extinction coefficient between version 5.1 and 5.2 . The ratio lower than 1 in Figure **??**c suggests enhanced extinction coefficient in version 5.2, which occurs due to the retention of data in the vicinity of the tropopause, whereas in version 5.1 these data points were removed due to the usage of a simple extinction ratio filter.

3.2 Revisiting GloSSAC

A detailed description of the various measurements used in constructing GloSSAC (v 2.0) is shown in Figure 1 of Kovilakam et al. (2020). An interim version of GloSSAC was recently released (v 2.1) for which the new aerosol/cloud categorization described in section 2.2 3.2 was implemented, without initial filtering of spurious negative values in the events as described in section 1.1 3.1. In version 2.1 of GloSSAC, the data were extended to through 2020. We now extend extended data through 2021 as data from individual measurements become became available for the year 2021. However, for the current version (v 2.2), there is no change in the individual measurements used but there are version changes in each data set in addition to the cloud-screening of SAGE III/ISS data as described above. The version changes of individual data sets are applicable only for the post-SAGE II era (September 2005- present) that now include a version change in SAGE III/ISS data as described in Section 1.1 section 2 with version changes in OSIRIS and CALIOP Optical Spectrograph and InfraRed Imaging System (OSIRIS) and Cloud-Aerosol Lidar and Infrared Pathfinder Satellite Observation (CALIPSO) as described below.

We now use OSIRIS version 7.2 data compared to version 7.0 used in GloSSAC (v 2.0). For OSIRIS version 7.2, the background atmosphere was changed from ERA-interim to MERRA2 re-analysis for consistency, and failures and missing data were also fixed so that there are now more scans in general. Overall, there are no significant differences between version 7.0 and 7.2, particularly above the UTLS region. Due to a decline in the coverage of the instrument, data for the month of June of 2018 through 2021 are now absent from the entire data set. Please note that due to inclusion of additional scans, the version 7.2 data now includes an increased number of profiles compared to version 7.0, which also results in differences between version 7.0 and 7.2. These differences are apparent, particularly in the high latitude bands. Additionally, in version 7.2, NO_2 regularization and ozone cross-section have been changed (personal communication, Adam Bourassa).

CALIPSO aerosol backscatter measurements have been valuable for GloSSAC, particularly in filling the gaps in the measurements, mostly in the polar latitudes. We use CALIPSO's Cloud-Aerosol Lidar with Orthogonal Polarization (CALIOP) aerosol backscatter coefficient data, which has also undergone a minor change to version 1.01 from July 2020, which is due to

an upgrade required to the operating system on the production cluster (https://www-calipso.larc.nasa.gov/resources/calipso_users_guide/data_quality/level_all_v001_20201002.php). ~~For the year 2021,~~ CALIOP data were available only ~~till~~ until October 2021. We, therefore used only the data that were available at the time of the analysis.

Here, we follow the methods described in Kovilakam et al. (2020) for merging OSIRIS, CALIOP, and SAGE III/ISS into the GloSSAC data set. For this version (v2.2) of GloSSAC, we update the dataset ~~post -2005~~ post-2005 for which there are version changes on all ~~the~~ three individual data sets that are used (i.e. OSIRIS, CALIOP, and SAGE III/ISS). While the measurements of OSIRIS and CALIOP provide most of the data in GloSSAC for the period from 2005 through mid 2017, it may also be noted that there are changes in instruments and fundamental ~~change~~ changes in the measurements as noted previously (e.g. Thomason et al., 2018; Kovilakam et al., 2020). While OSIRIS and CALIOP instruments use a less direct technique compared to solar occultation, these instruments provide greatest density of measurements. However, OSIRIS and CALIOP have challenges in retrieving aerosol properties. For OSIRIS, the retrieved aerosol extinction at 750 nm depends on an estimation of the aerosol scattering phase function~~estimation ,~~ which is related to aerosol size distribution and composition. CALIOP's primary measurement is backscatter coefficient which is measured at 532 nm. While CALIOP provides high density measurements even in the polar latitudes, ~~there~~ it appears to have poor precision on individual measurements in the stratosphere. Therefore, we use averaging of individual measurements to provide a precise product comparable to those provided by OSIRIS or SAGE when incorporating the ~~data set~~ dataset into GloSSAC. ~~Since~~ Further, since the GloSSAC aerosol extinction coefficients are provided at 525 and 1020 nm, the conversion from the CALIOP backscatter coefficient to extinction coefficient is another source of bias. A detailed description on biases related to individual instruments and their possible corrections is provided in Kovilakam et al. (2020).

3.2 ~~Comparison of SAGE III/ISS data with OSIRIS~~

3.1.1 Comparison of SAGE III/ISS data with OSIRIS

The primary wavelength at which OSIRIS extinction coefficient is retrieved is 750 nm. ~~We, therefore~~ Therefore, we need to convert the 750 nm extinction to the GloSSAC wavelengths which are at 525 and 1020 nm. Generally, the conversion to 525 nm is made using a constant Ångström exponent of 2.33 as noted in Rieger et al. (2015). While the comparison between OSIRIS and SAGE measurements are broadly in agreement, there appears to have been an overestimation of OSIRIS extinction in the lower stratosphere when compared against SAGE II and SAGE III/ISS (e.g. Rieger et al., 2015; Thomason et al., 2018; Kovilakam et al., 2020). Figure 11 shows zonally averaged monthly extinction coefficient percentage difference between OSIRIS and SAGE III/ISS for June 2017. For Figure 11a, the OSIRIS extinction at 525 nm is computed using a constant Ångström exponent of 2.33, whereas in Figure 11b the measurement is compared for 750 nm SAGE III/ISS measurement. Figure 11a,b show a reasonable agreement between OSIRIS and SAGE III/ISS except in the lower stratosphere and in the tropics where the percent difference exceeds 40 %. While Figure 11a shows the same patterns as in Figure 11b, the differences are significantly larger, which suggests either a deficiency in the conversion process of OSIRIS extinction from 750 to 525 or SAGE III/ISS is biased low in the lower and middle stratosphere. Therefore, to maintain ~~a~~ long-term consistency between ~~the data sets~~datasets,

it effectively requires that we bring OSIRIS in agreement with SAGE measurements. Following Kovilakam et al. (2020), a conformance process is performed to mitigate the differences between OSIRIS and SAGE measurements using a monthly climatology of pseudo Ångström exponent ~~. A detailed description of this method is available in Kovilakam et al. (2020)0pt.~~ (pseudo Ångström exponent is derived using monthly mean Ångström exponent as described in Kovilakam et al. (2020)0pt).

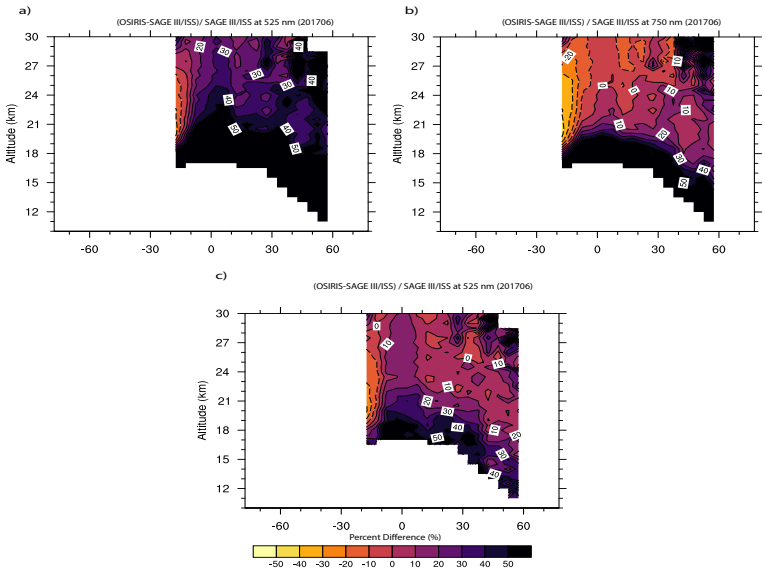

Figure 11. Percent difference between OSIRIS and SAGE III/ISS altitude versus latitude for June 2017 (a) at 525 nm , and (b) 750 nm. Ångström exponent of 2.33 is used to convert OSIRIS extinction to 525 nm in (a) while a monthly climatology of Ångström exponent from Figure 12 is used to convert OSIRIS extinction in (c).

While we follow the method provided in Kovilakam et al. (2020) for conforming OSIRIS data using pseudo Ångström monthly climatology, it is to be noted that we now include additional measurements available from OSIRIS and SAGE III/ISS from 2018 through ~~2020~~ 2021 to compute the monthly Ångström climatology. As noted in section ~~3.1~~ 3.1, there are version changes in both ~~the~~ data sets that now introduce differences in the Ångström climatology, which is used for the conformance process. Figure 12 shows the pseudo Ångström exponent monthly climatology ~~that are~~ on altitude versus latitude basis, which was computed using 750 nm OSIRIS and 525 nm SAGE II and SAGE III/ISS data. The difference between Figure 12 and Figure 7 of Kovilakam et al. (2020) arises mostly due to the relatively less comparable data between OSIRIS and SAGE III/ISS for GloSSAC version 2.0, where OSIRIS did not have data processed for the year 2018. Here, we now have additional data available from January 2018 through December 2021 from both OSIRIS and SAGE III/ISS and it should also be noted that both data sets have undergone small version changes, which may have also contributed toward the differences in Figure 12 in comparison with Figure 7 of Kovilakam et al. (2020).

~~Figure 11 shows a comparison measurement between OSIRIS and SAGE III/ISS for June 2017. For Figure 11a, the OSIRIS extinction is computed using~~ While the standard conversion of OSIRIS 750 to 525 nm uses a constant Ångström exponent

of 2.33, ~~whereas in Figure 11b the measurement is compared for 750 nm SAGE III/ISS measurement. Figure 11a,b show a reasonable agreement between OSIRIS and SAGE III/ISS except in the lower stratosphere and in the tropics where the percent difference exceeds 20 %. While Figure 11a shows same patterns as in Figure 11b, the differences are significantly larger in comparison with Figure 11b which suggests either a deficiency in the conversion process of OSIRIS extinction from 750 to 525 or SAGE III/ISS is biased low in the lower and middle stratosphere. Overall, the comparison of OSIRIS shows reasonable agreement except in the lower stratosphere where OSIRIS data appears to have a high bias relative to SAGE III/ISS measurements~~ Figure 12 shows values range from 1 through 4 for much of the stratosphere with exceptions in the tropical lower stratosphere. ~~Therefore, to maintain long-term consistency between data sets, a conformance process is performed using a monthly climatology of~~ It should be noted that the pseudo Ångström exponent shown in Figure 12 does not have any physical meaning as it accounts for potential deficiencies in both data sets and it is simply a means to push OSIRIS extinction measurements toward the measurements produced by SAGE. We, therefore use pseudo Ångström exponent ~~to convert OSIRIS extinction from~~ data shown in Figure 12 to convert zonally averaged monthly extinction of 750 nm OSIRIS to 525 ~~nm. The conformance process is detailed in section 2.4 of Kovilakam et al. (2020)0pt.~~ as shown in Figure 11 c.

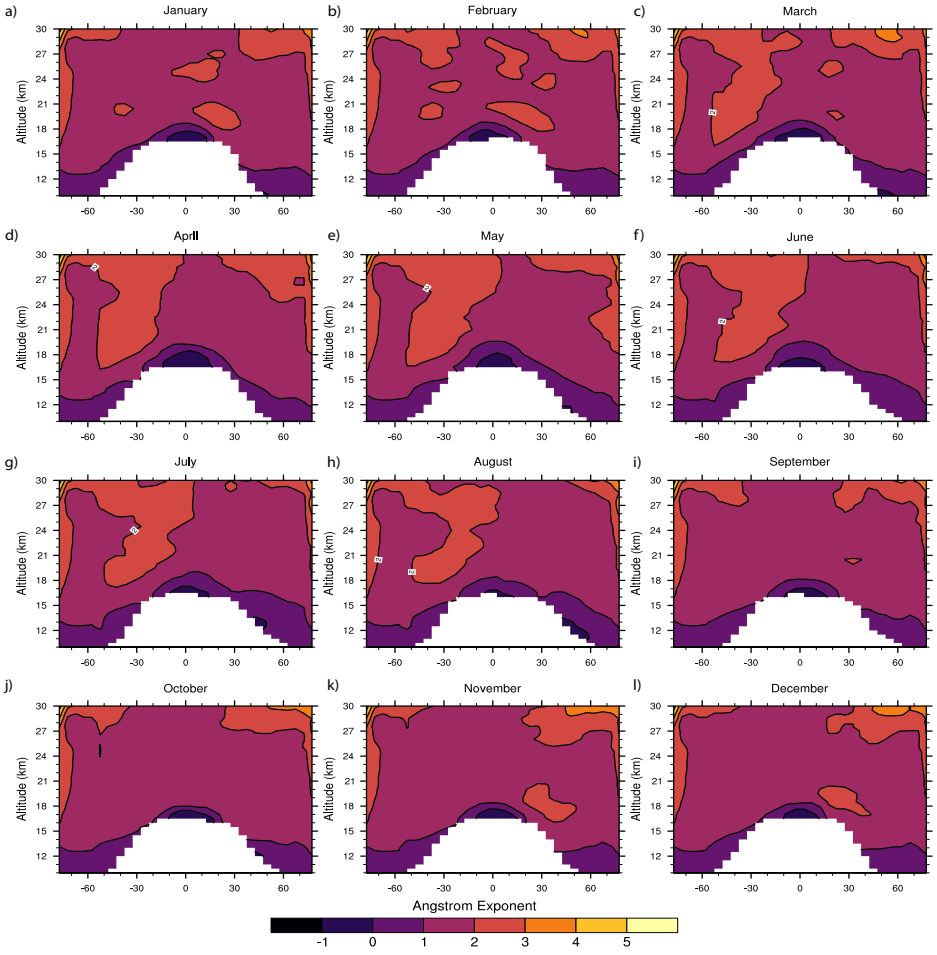

Figure 12. Altitude versus Latitude of Ångström exponent monthly climatology derived using OSIRIS 750 nm and SAGE II and SAGE III/ISS 525 nm extinction. Outliers are removed using 3x3 median smoothing. Please note that we apply linear interpolation to fill in missing data that are mostly applicable for the polar latitude (poleward of 55).

Figure 11c shows the comparison between bias corrected OSIRIS and SAGE III/ISS measurements. Figure 11c shows a significant improvement of OSIRIS extinction coefficient in the lower stratosphere where the differences are significantly reduced in comparison with Figure 11a. While this agreement looks better in Figure 11c for which the stratosphere is relatively less perturbed, there are some caveats as the usage of monthly climatology of pseudo Ångström exponent will be significantly different than the observed Ångström exponents, particularly following a perturbed event such as volcanic eruption or wildfire events. This becomes an issue for the period between SAGE II and SAGE III/ISS (August 2005 and June 2017) where we do not have any ~~mutli-wavelength~~ multi-wavelength measurements during which many small to moderate volcanic eruptions occurred.

Recently, it ~~is~~ has been shown that many small to moderate eruptions ~~can manifest themselves~~ were manifest during SAGE II and III/ISS data record (Thomason et al., 2021). The size information inferred from the 525 to 1020 nm extinction ratios show ~~that~~ a decrease in extinction ratio (increase in aerosol size) following large volcanic eruptions, whereas for small to moderate eruptions, extinction ratios are apparently slightly higher (smaller aerosol size) (Thomason et al., 2021). Therefore, we note that inferring aerosol size information for the post-SAGE II period (September 2005 through May 2017) is deficient, particularly following several small to moderate volcanic eruptions. We use ~~a similar conversion process~~ monthly climatology of pseudo Ångström exponent for converting OSIRIS extinction coefficient at 750 nm to 525 and 1020 as described in section 2.4 of Kovilakam et al. (2020). While this conversion process is a better step forward in combining data sets into a uniform data set, ~~we note that the pseudo Ångström exponent used for conformance does not have any physical meaning~~the conversion process may be deficient in addressing evolving size changes that affect extinction measurements following any perturbed event (Kovilakam et al., 2020)0pt.

3.2 ~~Comparison of SAGE III/ISS data with CALIOP and OSIRIS~~

3.1.1 Comparison of SAGE III/ISS data with CALIOP and OSIRIS

Here, we follow the same method used in Kovilakam et al. (2020) to incorporate CALIOP data into the GloSSAC data set. While CALIOP uses lidar to measure the aerosol backscatter coefficient at 532 nm, a source of bias occurs when backscatter coefficient is converted to extinction coefficient as the conversion process requires information of unknown aerosol composition and size distribution (Kar et al., 2019). Here, we use the CALIOP standard stratospheric aerosol data product (Kar et al., 2019), with a minor version change from June 2020. For CALIOP data processing, a constant aerosol extinction-to-backscatter ratio of 50 sr is used (Kar et al., 2019) ~~. CALIOP~~ and the standard aerosol extinction is reported at 532 nm. Therefore, a constant Ångström exponent of 2.33 is used to convert extinction coefficient to 525 nm. Figure 13a,b show percent differences between standard CALIOP extinction coefficient and bias corrected OSIRIS and SAGE III/ISS extinction coefficient at 525 nm for November 2017. CALIOP ~~is~~ extinction in Figure 13a,b is computed using a constant extinction-to-backscatter ratio of 50. CALIOP is in reasonable agreement with OSIRIS and SAGE III/ISS except in the lower stratosphere and at higher latitudes ($> 50°$), where the differences are larger than 50 %. While we can attribute some of these differences in the northern higher latitudes to PyroCb event associated with Canadian wildfire (Peterson et al., 2018), we note that similar differences persist even when the stratosphere is in the quiescent state. We, therefore use a conformance method described in Kovilakam et al. (2020) to reduce the bias between measurements. Following Kovilakam et al. (2020), we implement an empirical scale factor (SF) which is computed as the ratio of bias corrected OSIRIS extinction at 525 ~~m~~ nm to CALIOP backscatter coefficient at 532 nm. As noted in Kovilakam et al. (2020), we re-derive the backscatter using attenuated scattering ratio and molecular backscatter due to the fact that the standard aerosol backscatter coefficient is retrieved using a lidar ratio of 50 sr (Kar et al., 2019). For GloSSAC (v2.2), we use this alternate backscatter coefficient ~~same as the method used in GloSSAC v2.0~~the same way as in Kovilakam et al. (2020)0pt.

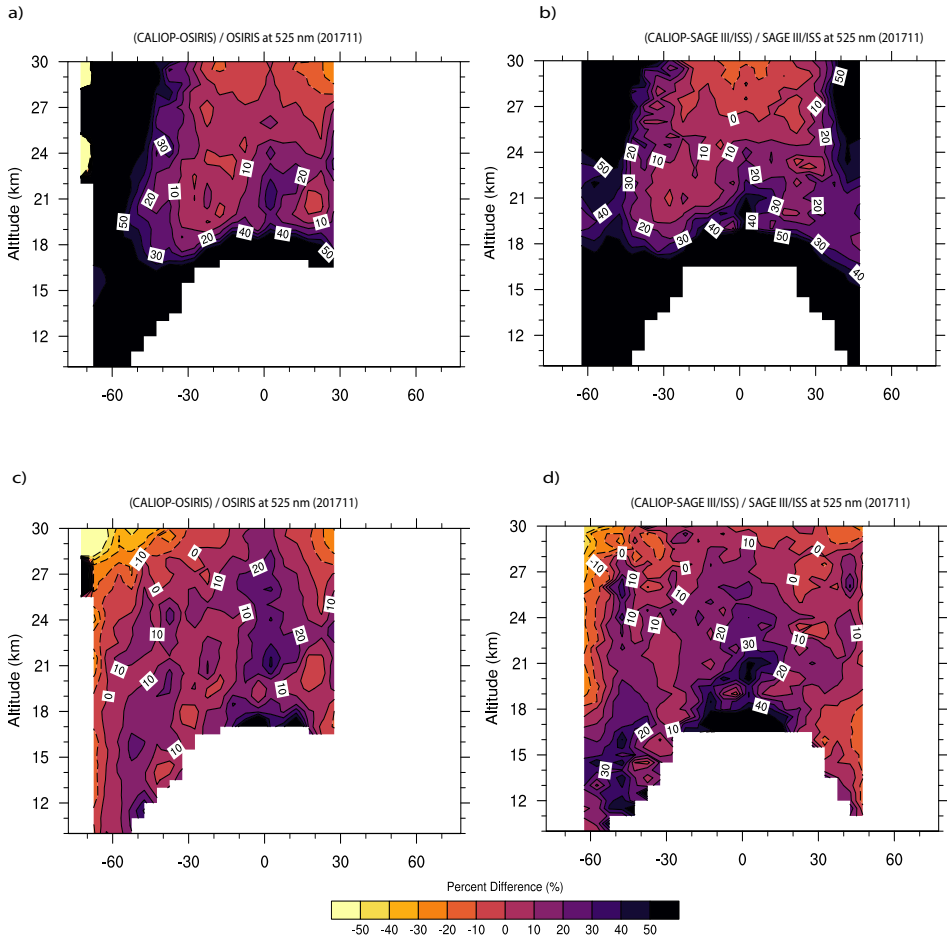

Figure 13. Percent difference between CALIOP, bias corrected OSIRIS, and cloud screened SAGE III/ISS extinction coefficients for November 2017. CALIOP data used in (a) and (b) are for 532 nm available in CALIOP stratospheric aerosol product, whereas CALIOP data in (c) and (d) are bias corrected using the scale factor (SF) showed in Figure 14a.

Figure 14a depicts ~~that annual median of~~ the annual median SF on an altitude versus latitude basis. Figure 14a suggests that the SF values range from 10 at polar latitudes to about 65 in the tropical high altitudes. While SF in Figure 14a is in reasonable agreement with Figure 9 of Kovilakam et al. (2020), the differences in Figure 14 can be attributed to version changes and the additional measurements available from 2018 through 2021. Figure 14b shows the relative standard deviation for the SF in Figure 14a ~~that shows~~ and demonstrates that the SF is reasonably consistent except at polar latitudes where relative standard deviations are larger than 50 %. To compute the annual median ~~of~~ SF, we use data from 2006 through ~~2020~~ 2021 when both measurements are available on a monthly basis. We, then apply the conversion factors shown in Figure 14a to the entire CALIOP data set on an altitude versus latitude basis. This empirically scaled CALIOP 525 nm data is used for computing the percent difference plots shown in Figure 13c,d. It is evident from these plots that the differences between the data sets is

reduced and is mostly within ± 20 % when compared against Figure 13a,b for which the ~~differences~~ difference was ≥ 50 %. While the discrepancies between the data sets are reduced, they are not completely eliminated. We follow the same approach for converting CALIOP backscatter from 532 nm to 1020 nm extinction (not shown here). We plan to revise this method in a future version of GloSSAC as a time dependent SF can possibly be introduced after filling in missing values of OSIRIS and CALIOP monthly data using equivalent latitude.

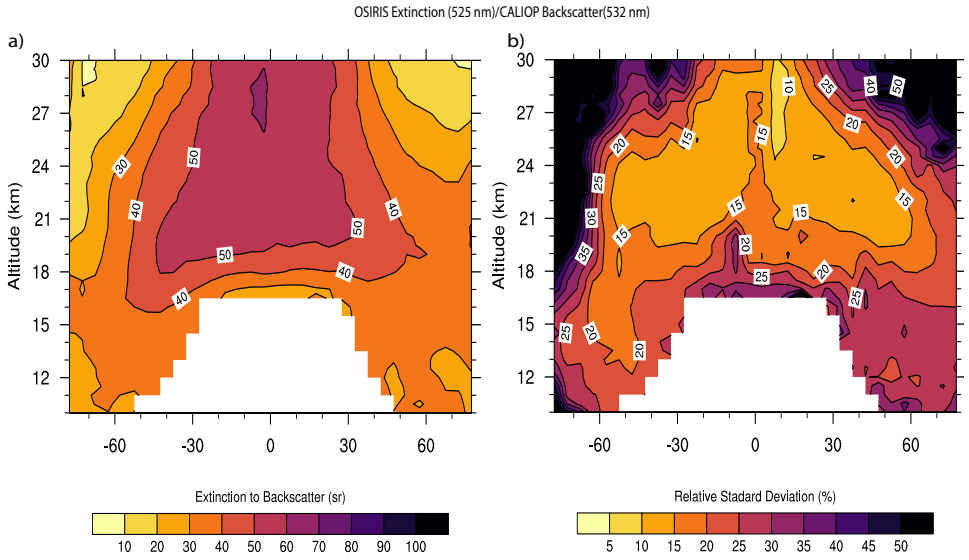

Figure 14. (a) Altitude versus latitude dependence of 525 bias corrected OSIRIS extinction to 532 CALIOP backscatter ratio (SF) for the overlap period between 2006 and 2021. (b) relative standard deviation of (a) is computed at each grid point with respect to the median value in percent.

4 Implications of cloud-screening on GloSSAC

For GloSSAC, SAGE III/ISS data is zonally averaged into 5°latitude bins, and 0.5 km altitude resolution on a monthly basis and incorporated into GloSSAC . Additionally, for version (v2.2), we perform a linear interpolation along the time axis to fill in missing values at higher latitudes. For a future release, we plan to implement a reconstruction method for SAGE III/ISS to fill in missing data— a method similar to the one used for SAGE II in GloSSAC version 1.0 (Thomason et al., 2018)0pt. It should also be noted that we now use version 5.2 SAGE III/ISS products in GloSSAC (v2.2) with revised cloud screening algorithm, whereas SAGE III/ISS version 5.1 was used in GloSSAC (v2.0) (Kovilakam et al., 2020)0pt. Figure 15 shows the impact of the revised cloud screening algorithm on SAGE III/ISS aerosol data. For the cloud screened product, we use three flags from the cloud screen algorithm, which are "Standard aerosol", "Perturbed aerosol", and "Enhanced Aerosol/Tropopause Cloud" respectively as shown in section 3.2.1. It should also be noted that, while we use 756 and 1544 nm wavelengths extinction ratio for the aerosol/cloud categorizations, the categorizations mentioned in section 3.2.1 are applied to all aerosol channels

from 384 through 1544 nm on the basis of 756/1544 nm extinction ratio. GloSSAC provides zonally averaged extinction coefficients at 525 and 1020 nm wavelengths for historical reasons. We therefore continue the same historical measurement wavelengths in the latest version of GloSSAC v 2.2. While we note the negative bias in 525 nm channel, a correction has been made to 525 nm channel by spectrally interpolating extinction between 450 and 756 nm channel using Ångström exponent (Knepp et al., 2021)0pt. It should also be noted that the bias between measured and Ångström exponent interpolated values due to the curvature in the spectra, is generally within $\pm$ 10% (Thomason et al., 2010)0pt.

Figure 15a,b shows zonally averaged altitude versus latitude plots of extinction coefficients at 525 nm for version 5.1 and 5.2 respectively. The impact of cloud screening is evident from Figure 15b with a clear enhancement in extinction coefficient in the latitudes $>$ 30°N, particularly in the lower stratosphere. The enhanced extinction in version 5.2 is further evident from Figure 15c, which shows the ratio of extinction coefficient between version 5.1 and 5.2 . Figure 15c shows lower range of ratios from 0.40 to 0.6, between 37.5°N and 57.5°N latitudes and at altitudes between 17 and 19 km (marked with a black oval in Figure 15c). Lower ratios suggest enhanced extinction coefficient in version 5.2, which occurs due to the removal of extinction coefficient data points with extinction ratios $<$ 2.0 in version 2.0. Additionally, for version 5.2, we perform a linear interpolation along the time axis to fill in missing values at higher latitudes, which can be seen in Figure 15b.

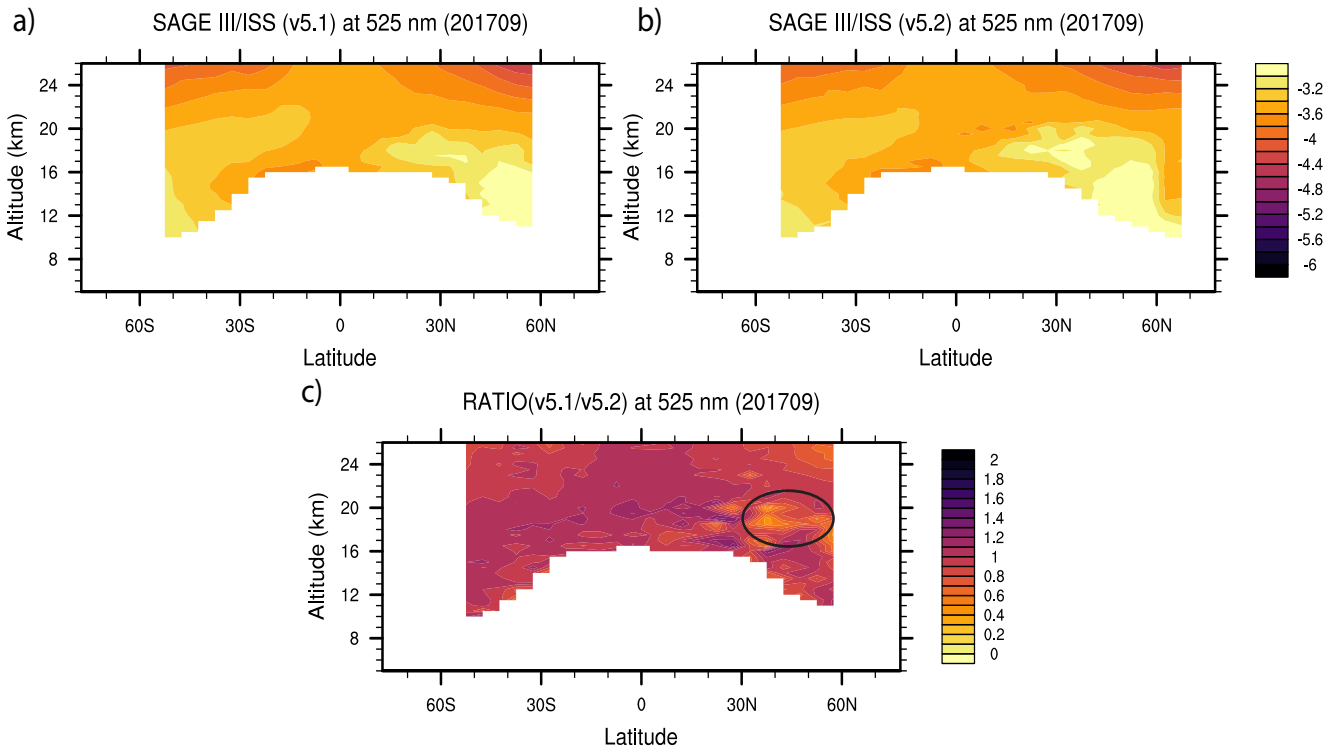

Figure 15. Zonally averaged SAGE III/ISS altitude versus latitude extinction coefficients for September 2017 following the Canadian wildfire event. (a) version 5.1 (b) for version 5.2 and (c) ratio between version 5.2 and 5.1. Extinction coefficient values are shown in the log to base 10.

4.1 Comparison of GloSSAC version 2.2 with version 2.0

To construct the GloSSAC data set, all individual measurements are gridded to the GloSSAC resolution (monthly, 0.5 km altitude and 5 degree latitude resolution). As previously done for GloSSAC v2.0, from June 2017, we prioritize SAGE III/ISS data over OSIRIS and CALIOP. For the post-2017 data, several small to moderate volcanic events and a few large wildfire events have been reported (Table 1). It is therefore important to compare the differences between version 2.2 and version 2.0 of the GloSSAC data set. Figure ~~??~~ 16 shows extinction coefficient for September 2017, following ~~Canadian wildfire. Figure ?? a shows the GloSSAC (v~~ the Canadian wildfire, for version 2.0 ~~) 525 nm extinction coefficient for September 2017, while Figure ?? b shows extinction coefficient for GloSSAC version~~ and 2.2~~. The ratios between Figure ?? a, and b are shown in Figure ??c~~, as well as the ratios. It is ~~clearly~~ evident from Figure ~~?? c~~ 16i that the revised cloud screen method used in v2.2 ~~that apparently~~ retains extinction data in the lower stratosphere that ~~were~~ was otherwise removed in version 2.0 because of a simple extinction ratio filter— thereby enhancing aerosol extinction in version 2.2 for the latitude band between 35 and 50°N ~~.~~ ~~The differences in the~~ for altitudes between 17 and 19 km (marked with a black oval in Figure 16i). Lower ratios in Figure 16i suggest enhanced extinction coefficient in version 2.2, which occurs due to the removal of extinction coefficient data points

with extinction ratios $\leq$ 2.0 in version 2.0. The differences we see in Figure 16i is same as in Figure 15c for the latitudes between 50°S and 50°N, for which SAGE III/ISS data are used. The differences in the polar latitudes ($>$ 60°) in version 2.2 could be attributed to changes that occurred in individual data sets in version 2.2 as shown in Figure 16~~. Additionally~~a-f. For the southern polar latitudes (poleward of 60°S), the differences ~~in the polar latitudes could be a result of a~~ are mainly due to the version changes in the individual data sets, particularly from OSIRIS and CALIOP as shown Figure 16 a-d. However, for the northern polar latitudes (poleward of 60°N), the difference could be attributed to both version changes in the individual sets as well as a linear interpolation scheme ~~in time~~ performed for SAGE III/ISS data in GloSSAC v2.2 to fill in missing values.

5 ~~Stratospheric Aerosol Optical Depth~~

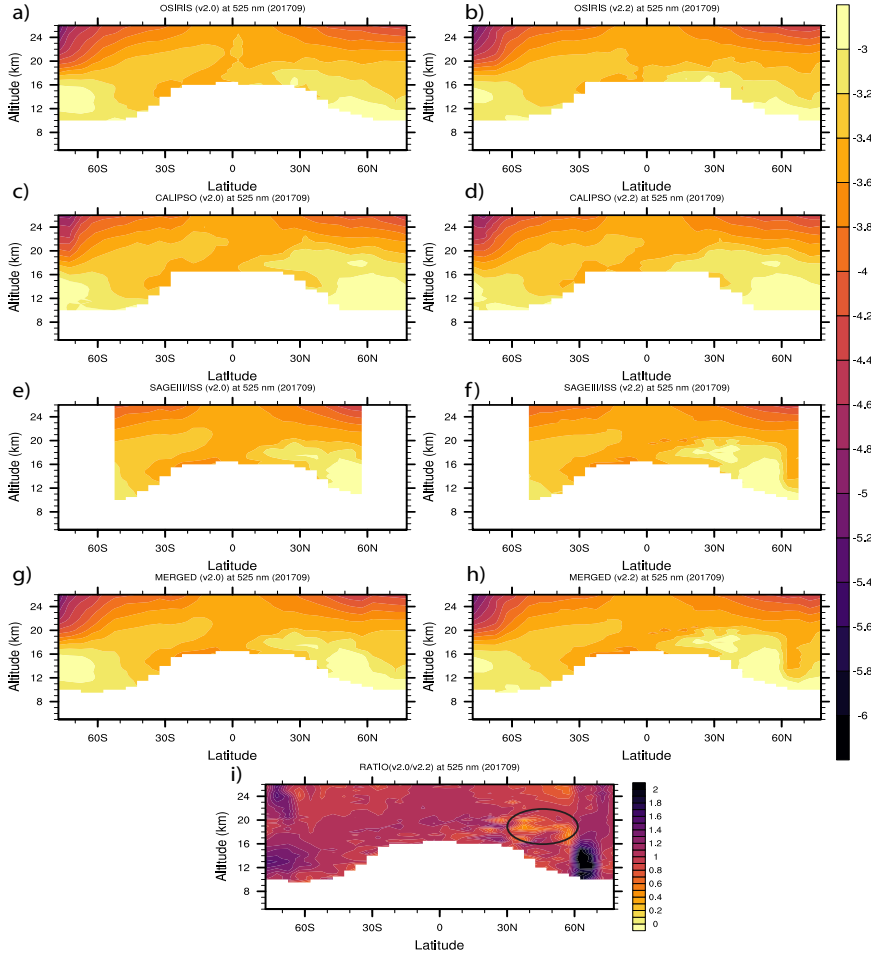

Figure 16. Altitude versus latitude dependence of 525 nm extinction for September 2017. (a,c,e,g) for OSIRIS, CALIOP, SAGE III/ISS, and merged extinction for version 2.0 respectively, whereas (b,d,f,h) are for version 2.2. (i) shows the ratio between merged version 2.2 (h) and 2.0 (g).

4.1 Stratospheric Aerosol Optical Depth

Stratospheric aerosol optical depth (SAOD) was incorporated as a separate variable in all previous versions of GloSSAC and therefore, we incorporate SAOD into GloSSAC version 2.2. Figure 17 shows zonally averaged monthly latitude versus time of SAOD for GloSSAC version 2.0 and version 2.2. While the data in version 2.0 and 2.2 remains the same for the period prior to 2005, there are differences between the versions for the post-2005 time period. ~~It is worthwhile to note here that OSIRIS data used in version 2.2 has undergone minor changes with additional measurements included that affects the data broadly~~

but more so in the polar latitudes. This may have caused differences for Therefore, we only show AOD changes post-2005 in Figure 17. While the differences in SAOD at 525 nm SAOD in version and 1020 nm between version 2.0 and 2.2 of GloSSAC, particularly for the southern hemispheric polar latitudes , which is evident in are generally within ± 20% for latitudes between 60°S and 60°N, larger differences are noticeable in the high latitudes and the tropics, following the Canadian Wildfire event in 2017 and the Ambae volcanic eruption in 2018 (Figure 17c. Figure 17b,c show additional data from ,f). The lower extinction coefficients in GloSSAC v2.2 in the polar latitudes could be attributable to the changes occurred to individual data sets due to version changes. However, the enhanced extinction in GloSSAC (v2.2) followed by Canadian Wildfire event in July 2017 and Ambae volcanic eruption in 2018through 2021 , is attributable to new aerosol/cloud categorization in version 2.2 , suggesting increased stratospheric aerosol loading due to several volcanic eruptions and wildfire events that are listed in Table 1. Globally averaged SAOD shows the differences between that retains lower stratospheric data, while GloSSAC version 2.0 used a simple extinction ratio based cloud filter that could have removed more aerosol data that have extinction ratios < 2.0. While larger percent differences are observed following the Canadian Wildfire in July 2017 for 1020 nm (percent difference as large as -52% for the latitudes between 50°N and 57.5°N), relatively smaller percent difference is observed for 525 nm (percent difference as large as -31% for the latitudes between 50°N and 57.5°N). As far as the differences in extinction coefficient following the Ambae volcanic eruption in July 2018 is concerned, both 525 and 1020 nm wavelengths show larger percent difference in the tropical latitudes (percent difference is as large as -37% (-47%) for 525 nm (1020 nm), for the latitudes between 20°S and 10°N). However, these differences between version 2.0 and 2.2 are generally within 20 %much lower (within 10 %) for globally averaged SAOD (Figure 18). Additionally, we note the impact of SAGE III/ISS cloud screening on GloSSAC version 2.2, which now shows an enhancement of aerosol extinction in comparison to version 2.0 following Canadian Wildfire event (July 2017) and Ambae volcanic eruption (July 2018). This is clearly evident in the percent difference plots shown in Figure 17 and While the difference is much smaller in the globally averaged SAOD time series, Figure 18 at both 525 and 1020 nm channels respectivelyb,d clearly shows decreases in percent difference of SAOD following the Canadian Wildfire event in July 2017 and the Ambae volcanic eruption in July 2018, suggesting higher extinction coefficients in version 2.2.

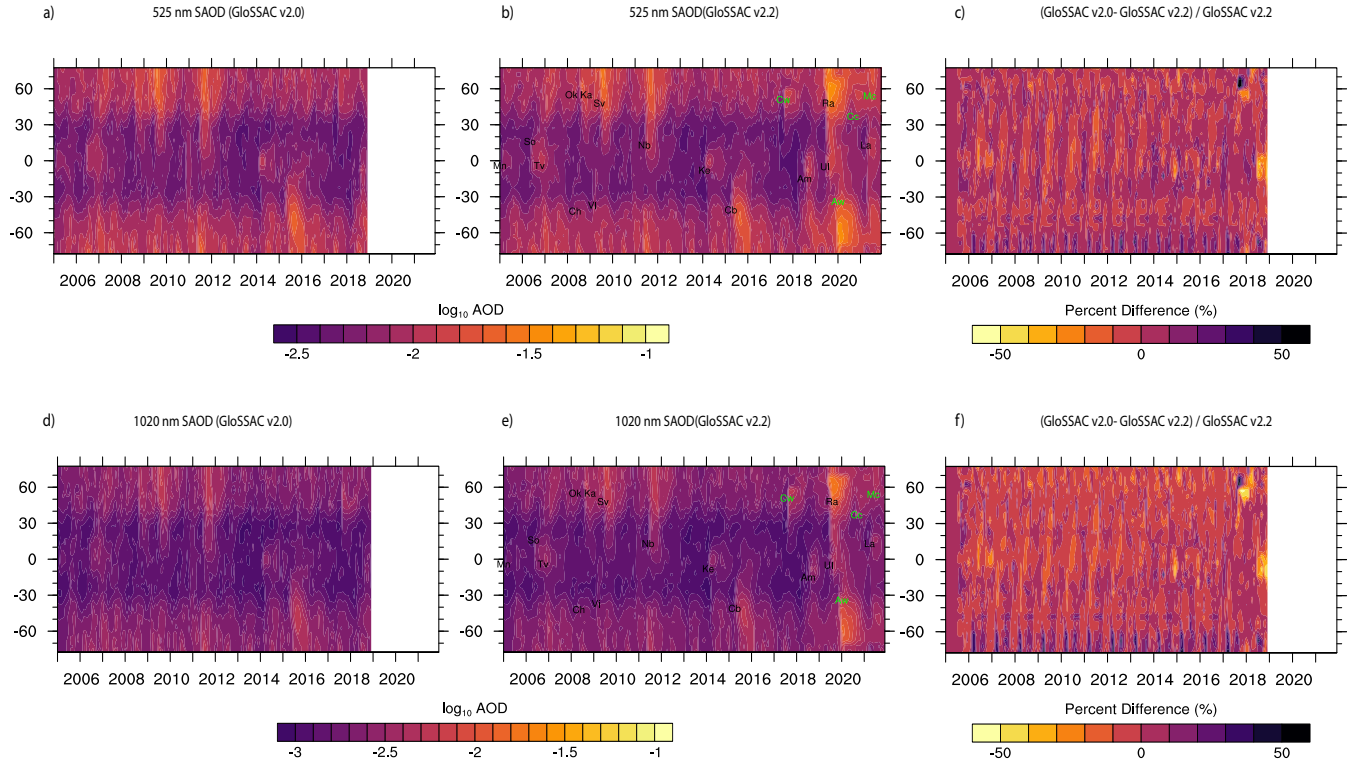

Figure 17. Latitude versus time dependence of SAOD for 525 and 1020 nm. (a,b,c) SAOD for 525 nm for GloSSAC version 2.0, version 2.2, and percent difference between (a) and (b). (d,e,f) Same as in (a,b,c) but for 1020 nm. (b, e) show major volcanic eruptions (black) and wild fire events (green) with abbreviated two letter code with their respective latitude and time of occurrence that are listed here. The event names shown in figures are: Manam (Mn), Soufriere Hills (So), Tavurvur (Tv), Chaiten (Ch), Okmok (Ok), Kasatochi (Ka), Sarychev (Sv), Nabro (Nb), Kelut (Ke), Calbuco (Cb), Canadian Wildfires (Cw), Ambae (Am), Ulawun (Ul), Australian Wildfire (Aw), California Creek Fire (Cc), La Soufriere (La), McKay Creek Fire (Mc).

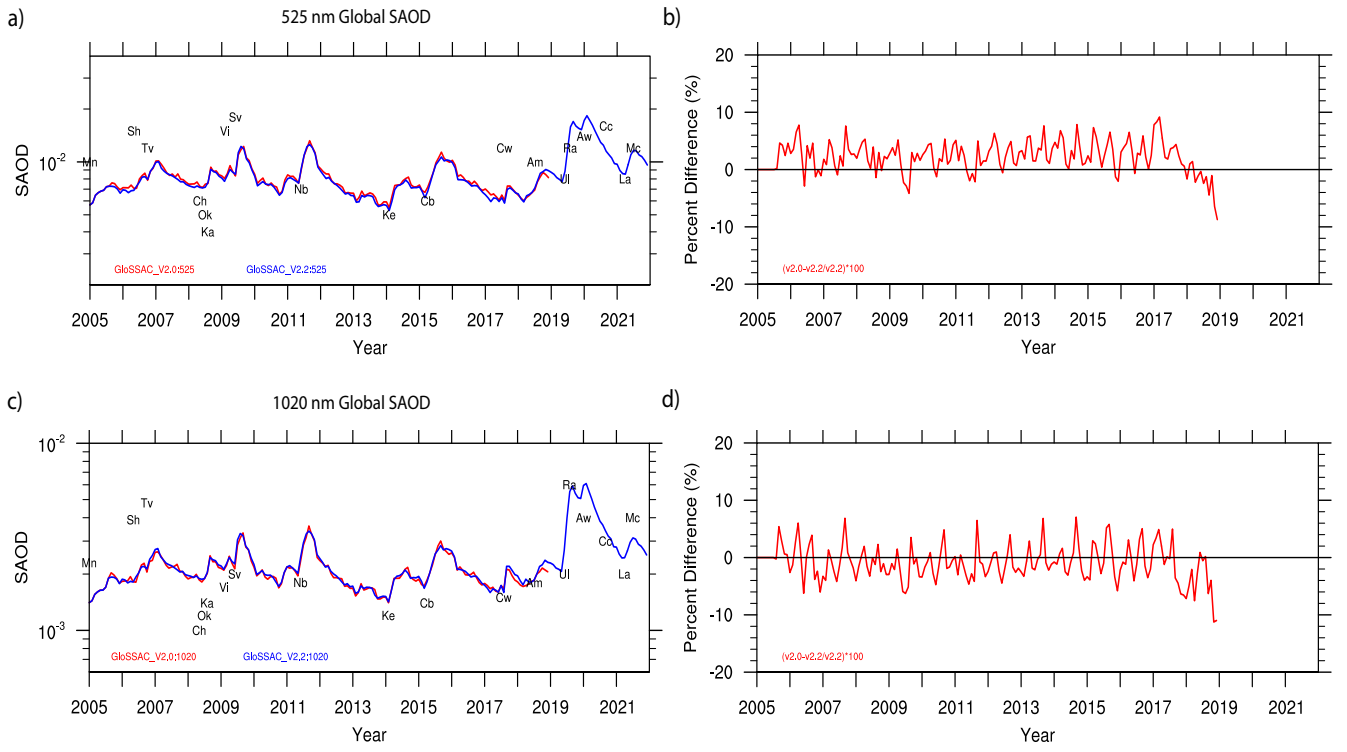

Figure 18. Time series of globally averaged SAOD for 525 and 1020 nm. Percent difference between version 2.0 and 2.2 are shown in (b,d) for 525 and 1020 nm.

5 Conclusions

~~We developed a revised~~

We developed the SOATCM method to categorize aerosol and clouds using SAGE III/ISS measurements. The primary goal behind ~~a revised cloud filtering method~~ SOATCM was to account for the influence of recent volcanic eruptions and PyroCb events on stratospheric aerosol loading in SAGE III/ISS measurements. ~~The revised method~~ Eventually, the SOATCM method will be used to produce a level 3 SAGE III/ISS aerosol product. The SOATCM works reasonably well for the periods during and following perturbed events such as volcanic/PyroCb. The influence of any perturbed activity in the stratosphere is estimated from the monthly time series of k_0, which is computed using median absolute deviation statistics and is now incorporated in the algorithm so that analyses that fall in this time frame is considered as "Perturbed" due to enhancement in k_0 value when compared against the "~~background~~standard" aerosol. Additionally, we use temperature based tropopause to classify the aerosols that are present in the vicinity of the tropopause which ~~is~~ are otherwise flagged as "aerosol/cloud mixture".

The implications of the revised cloud screen algorithm on GloSSAC data is also described. While there is no difference in the data prior to September 2005, the post-SAGE II era (September 2005-May 2017) clearly suggests differences between

GloSSAC v 2.0 and this version (v 2.2). The differences between v2.0 and 2.2 are mostly attributable to version changes in the individual data sets, and revised cloud screening method used for SAGE III/ISS in v 2.2 of GloSSAC. While all individual data sets for post-SAGE II era underwent version changes, the changes to OSIRIS is perceptible due to the increased number of measurements in the latest version of OSIRIS (v7.1) which causes differences in the zonally averaged data for GloSSAC v2.2. While the differences are relatively low (≤ 20 %) except for the polar latitude for the period between post-SAGE II era and SAGE III/ISS era (June 2017- present), the difference between v2.0 and 2.2 of GloSSAC is relatively larger, particularly in the lower stratosphere following any perturbed events for the SAGE III/ISS time period (June 2017-present) which is attributable to the revised cloud screen algorithm that now retains data in the ~~vicinity of the tropopause~~ lower stratosphere that was otherwise omitted with a simple extinction ratio based cloud screening in GloSSAC v2.0. The differences at the polar latitudes could be attributed to both version changes in individual data sets and the time interpolation of SAGE III/ISS data that is now implemented in version 2.2 due to discrepancies between data sets at the polar latitudes. While the same is true for SAOD where the time series of SAOD clearly shows the enhancement of SAOD following perturbed events, it is also noticeable that the enhancement of SAOD in the southern polar latitude that was present in all previous versions of GloSSAC is now diminished, although not completely. The improvements in SAOD in the polar latitudes could be attributable to increased number of measurements available in the latest version of OSIRIS (v7.2) and thereby improved zonal averaging for those latitude bands. Additionally, in GloSSAC v2.2, a time interpolation of SAGE III/ISS data is now implemented which may have caused some differences at the higher latitude as well. We also note that there are slight differences between the interim version 2.1 and this version (v 2.2) of GloSSAC (not shown here), as our aerosol/cloud categorization in both the versions remain ~~relatively~~ the same except that in version 2.2, an initial filtering of spurious negative values in the SAGE III/ISS events is implemented as described in section ~~1.1~~ 3.1. Additionally, in GloSSAC 2.2, OSIRIS version changes from 7.1 to 7.2.

While there are noticeable improvements in GloSSAC v2.2, we plan to implement some changes in future that are listed below.

- We plan to revisit the way smoke events are represented in GloSSAC during SAGE II era. We plan to consider the possibility of not using any cloud clearing for SAGE II data sets just above the tropopause except in seasons with PSCs. It is likely that the current method is removing smoke aerosol data from SAGE II in the lower stratosphere due to a mix up with clouds particularly in the vicinity of the tropopause. We are currently revisiting this method to identify smoke events for SAGE II. In light of the new insights in the development of this new technique, we will likely revisit cloud detection used for the SAGE II in the production of the GloSSAC data set.

- We plan to include an improved scale factor for OSIRIS extinction to CALIOP backscatter ratios, and estimation of Ångström exponent from OSIRIS and SAGE III/ISS to convert OSIRIS 750 nm extinction to 525 and 1020 nm. Despite improvements in the data for the post-SAGE II era in GloSSAC across the versions, we understand the limitations of the conversion method used particularly during periods when the stratosphere is perturbed due to volcanic and PyroCb activities. For CALIOP extinction estimation at 525 and 1020 nm from backscatter coefficient at 532 nm, we plan to implement a time dependent scale factor that will be computed after filling in OSIRIS and CALIOP missing values

at higher latitudes with equivalent latitude approach which was implemented for the SAGE II data in GloSSAC. A similar equivalent latitude approach can be implemented for SAGE III/ISS data that will improve estimation of Ångström exponent on a monthly basis which could then be used to convert OSIRIS 750 nm extinction to 525 and 1020 nm for the post-2017 data set.

Data availability. The GloSSAC v2.2 netCDF file is available from the NASA Atmospheric Data Center (https://asdc.larc.nasa.gov/data/GloSSAC/GloSSAC_V2.2.nc) (NASA/LARC/SD/ASDC, 2022). The SAGE III/ISS and CALIOP data used in this study are available from NASA Atmospheric Data Center, while OSIRIS version 7.2 data are downloaded from https://arg.usask.ca/docs/osiris_v7.

Author contributions. MK and LWT developed the idea and methodology used in this paper. MK carried out the analysis, while TK participated in the scientific discussion. MK wrote the manuscript, while all authors reviewed the manuscript and provided advice on the manuscript and figures.

Competing interests. The authors declare that they have no conflict of interest.

Acknowledgements. We acknowledge the support of NASA Science Mission Directorate and the SAGE II and III/ISS mission teams. The SAGE mission is supported by the NASA Science Mission Directorate. SSAI personnel are supported through the STARSS III contract.

References

Boothe, A. C. and Homeyer, C. R.: Global large-scale stratosphere–troposphere exchange in modern reanalyses, Atmospheric Chemistry and Physics, 17, 5537–5559, https://doi.org/10.5194/acp-17-5537-2017, 2017.

Bourassa, A. E., Robock, A., Randel, W. J., Deshler, T., et al.: Large volcanic aerosol load in the stratosphere linked to Asian monsoon transport, Science, 337, 78–81, 2012.

Bourassa, A. E., Rieger, L. A., Zawada, D. J., Khaykin, S., Thomason, L. W., and Degenstein, D. A.: Satellite Limb Observations of Unprecedented Forest Fire Aerosol in the Stratosphere, Journal of Geophysical Research: Atmospheres, 124, 9510–9519, https://doi.org/10.1029/2019JD030607, 2019.

Deshler, T., Hervig, M. E., Hofmann, D. J., Rosen, J. M., and Liley, J. B.: Thirty years of in situ stratospheric aerosol size distribution measurements from Laramie, Wyoming (41°N), using balloon-borne instruments, Journal of Geophysical Research: Atmospheres, 108, https://doi.org/https://doi.org/10.1029/2002JD002514, 2003.

Deshler, T., Luo, B., Kovilakam, M., Peter, T., and Kalnajs, L. E.: Retrieval of Aerosol Size Distributions From In Situ Particle Counter Measurements: Instrument Counting Efficiency and Comparisons With Satellite Measurements, Journal of Geophysical Research: Atmospheres, 124, 5058–5087, https://doi.org/https://doi.org/10.1029/2018JD029558, 2019.

Eyring, V., Bony, S., Meehl, G. A., Senior, C. A., Stevens, B., Stouffer, R. J., and Taylor, K. E.: Overview of the Coupled Model Intercomparison Project Phase 6 (CMIP6) experimental design and organization, Geoscientific Model Development, 9, 1937–1958, https://doi.org/10.5194/gmd-9-1937-2016, 2016.

Fahey, D., Kawa, S., Woodbridge, E., Tin, P., Wilson, J., Jonsson, H., Dye, J., Baumgardner, D., Borrmann, S., Toohey, D., et al.: In situ measurements constraining the role of sulphate aerosols in mid-latitude ozone depletion, Nature, 1993.

Hervig, M. and Deshler, T.: Evaluation of aerosol measurements from SAGE II, HALOE, and balloonborne optical particle counters, Journal of Geophysical Research: Atmospheres, 107, AAC 3–1–AAC 3–12, https://doi.org/https://doi.org/10.1029/2001JD000703, 2002.

Hofmann, D. J. and Solomon, S.: Ozone destruction through heterogeneous chemistry following the eruption of El Chichon, J. Geophys. Res. Atmos, 94, 5029–5041, 1989.

Iglewicz, B. and Hoaglin, D.: How to Detect and Handle Outliers, ASQC basic references in quality control, ASQC Quality Press, 1993.

Kablick III, G. P., Allen, D. R., Fromm, M. D., and Nedoluha, G. E.: Australian PyroCb Smoke Generates Synoptic-Scale Stratospheric Anticyclones, Geophysical Research Letters, 47, e2020GL088 101, https://doi.org/https://doi.org/10.1029/2020GL088101, 2020.

Kar, J., Lee, K.-P., Vaughan, M. A., Tackett, J. L., Trepte, C. R., Winker, D. M., Lucker, P. L., and Getzewich, B. J.: CALIPSO level 3 stratospheric aerosol profile product: version 1.00 algorithm description and initial assessment, Atmospheric Measurement Techniques, 12, 6173–6191, https://doi.org/10.5194/amt-12-6173-2019, 2019.

Kaufman, L. and Rousseeuw, P. J.: Partitioning Around Medoids (Program PAM), John Wiley and Sons, Ltd, https://doi.org/https://doi.org/10.1002/9780470316801.ch2, 1990.

Kent, G. S. and McCormick, M. P.: Separation of cloud and aerosol in two-wavelength satellite occultation data, Geophysical Research Letters, 18, 428–431, https://doi.org/https://doi.org/10.1029/90GL02783, 1991.

Kent, G. S., Winker, D. M., Osborn, M. T., and Skeens, K. M.: A model for the separation of cloud and aerosol in SAGE II occultation data, Journal of Geophysical Research: Atmospheres, 98, 20 725–20 735, https://doi.org/https://doi.org/10.1029/93JD00340, 1993.

Kent, G. S., Wang, P.-H., and Skeens, K. M.: Discrimination of cloud and aerosol in the Stratospheric Aerosol and Gas Experiment III occultation data, Appl. Opt., 36, 8639–8649, https://doi.org/10.1364/AO.36.008639, 1997a.

Kent, G. S., Winker, D. M., Vaughan, M. A., Wang, P.-H., and Skeens, K. M.: Simulation of Stratospheric Aerosol and Gas Experiment (SAGE) II cloud measurements using airborne lidar data, Journal of Geophysical Research: Atmospheres, 102, 21 795–21 807, https://doi.org/https://doi.org/10.1029/97JD01390, 1997b.

Kloss, C., Berthet, G., Sellitto, P., Ploeger, F., Taha, G., Tidiga, M., Eremenko, M., Bossolasco, A., Jégou, F., Renard, J.-B., and Legras, B.: Stratospheric aerosol layer perturbation caused by the 2019 Raikoke and Ulawun eruptions and their radiative forcing, Atmospheric Chemistry and Physics, 21, 535–560, https://doi.org/10.5194/acp-21-535-2021, 2021.

Knepp, T., Thomason, L., Kovilakam, M., Tackett, J., Kar, J., Damadeo, R., and Flittner, D.: Identification of Smoke and Sulfuric Acid Aerosol in SAGE III/ISS Extinction Spectra Following the 2019 Raikoke Eruption, Atmospheric Measurement Techniques Discussions, 2021, 1–30, https://doi.org/10.5194/amt-2021-333, 2021.

Kovilakam, M., Thomason, L. W., Ernest, N., Rieger, L., Bourassa, A., and Millán, L.: The Global Space-based Stratospheric Aerosol Climatology (version 2.0): 1979–2018, Earth System Science Data, 12, 2607–2634, https://doi.org/10.5194/essd-12-2607-2020, 2020.

Legras, B., Duchamp, C., Sellitto, P., Podglajen, A., Carboni, E., Siddans, R., Grooß, J.-U., Khaykin, S., and Ploeger, F.: The evolution and dynamics of the Hunga Tonga–Hunga Ha'apai sulfate aerosol plume in the stratosphere, Atmospheric Chemistry and Physics, 22, 14 957–14 970, https://doi.org/10.5194/acp-22-14957-2022, 2022.

Manney, G. L., Hegglin, M. I., Lawrence, Z. D., Wargan, K., Millán, L. F., Schwartz, M. J., Santee, M. L., Lambert, A., Pawson, S., Knosp, B. W., Fuller, R. A., and Daffer, W. H.: Reanalysis comparisons of upper tropospheric–lower stratospheric jets and multiple tropopauses, Atmospheric Chemistry and Physics, 17, 11 541–11 566, https://doi.org/10.5194/acp-17-11541-2017, 2017.

Mauldin, L. E., Zaun, N. H., McCormick, M. P., Guy, J. H., and Vaughn, W. R.: Stratospheric aerosol and gas experiment II instrument:A functional description, Optical Engineering, 24, 307–312, https://doi.org/10.1117/12.7973473, 1985.

Minnis, P., Harrison, E., Stowe, L., Gibson, G., Denn, F., Doelling, D., and Smith, W.: Radiative climate forcing by the Mount Pinatubo eruption, Science, 259, 1411–1415, 1993.

NASA/LARC/SD/ASDC: Global Space-based Stratospheric Aerosol Climatology Version 2.2, https://doi.org/10.5067/GLOSSAC-L3-V2.2, 2022.

Palmer, K. F. and Williams, D.: Optical Constants of Sulfuric Acid; Application to the Clouds of Venus?, Appl. Opt., 14, 208–219, 1975.

Park, H.-S. and Jun, C.-H.: A simple and fast algorithm for K-medoids clustering, Expert Systems with Applications, 36, 3336–3341, https://doi.org/https://doi.org/10.1016/j.eswa.2008.01.039, 2009.

Peterson, D. A., Campbell, J. R., Hyer, E. J., Fromm, M. D., Kablick, G. P., Cossuth, J. H., and DeLand, M. T.: Wildfire-driven thunderstorms cause a volcano-like stratospheric injection of smoke, npj Climate and Atmospheric Science, 30, 2018.

Rieger, L. A., Bourassa, A. E., and Degenstein, D. A.: Merging the OSIRIS and SAGE II stratospheric aerosol records, J. Geophys. Res. Atmos., 120, 8890–8904, https://doi.org/10.1002/2015JD023133, 2015.

Rieger, L. A., Zawada, D. J., Bourassa, A. E., and Degenstein, D. A.: A Multiwavelength Retrieval Approach for Improved OSIRIS Aerosol Extinction Retrievals, Journal of Geophysical Research: Atmospheres, 124, 7286–7307, https://doi.org/10.1029/2018JD029897, 2019.

Rosen, J. M.: The Boiling Point of Stratospheric Aerosols, Journal of Applied Meteorology (1962-1982), 10, 1044–1046, http://www.jstor.org/stable/26175603, 1971.

Sellitto, P., Belhadji, R., Kloss, C., and Legras, B.: Radiative impacts of the Australian bushfires 2019–2020 – Part 1:Large-scale radiative forcing, Atmospheric Chemistry and Physics, 22, 9299–9311, https://doi.org/10.5194/acp-22-9299-2022, 2022a.

Sellitto, P., Podglajen, A., Belhadji, R., and et al.: The unexpected radiative impact of the Hunga Tonga eruption of 15th January 2022, Commun Earth Environ, 3, https://doi.org/10.1038/s43247-022-00618-z, 2022b.

SPARC: Assessment of Stratospheric Aerosol Properties (ASAP), Tech. rep., SPARC Report,WCRP-124,WMO/TD-No. 1295,SPARC Report No. 4, 348 pp., 2006.

Steele, H. M. and Hamill, P.: Effects of temperature and humidity on the growth and optical properties of sulphuric acid-water droplets in the stratosphere, Journal of Aerosol Science, 12, 517–528, 1981.

Thomason, L. W. and Vernier, J.-P.: Improved SAGE II cloud/aerosol categorization and observations of the Asian tropopause aerosol layer: 1989-2005, Atmospheric Chemistry and Physics, 13, 4605–4616, https://doi.org/10.5194/acp-13-4605-2013, 2013.

Thomason, L. W., Herber, A. B., Yamanouchi, T., and Sato, K.: Arctic Study on Tropospheric Aerosol and Radiation: Comparison of tropospheric aerosol extinction profiles measured by airborne photometer and SAGE II, Geophysical Research Letters, 30, https://doi.org/https://doi.org/10.1029/2002GL016453, 2003.

Thomason, L. W., Burton, S. P., Luo, B.-P., and Peter, T.: SAGE II measurements of stratospheric aerosol properties at non-volcanic levels, Atmos. Chem. Phys., 8, 983–995, 2008.

Thomason, L. W., Moore, J. R., Pitts, M. C., Zawodny, J. M., and Chiou, E. W.: An evaluation of the SAGE III version 4 aerosol extinction coefficient and water vapor data products, Atmospheric Chemistry and Physics, 10, 2159–2173, https://doi.org/10.5194/acp-10-2159-2010, 2010.

Thomason, L. W., Ernest, N., Millán, L., Rieger, L., Bourassa, A., Vernier, J.-P., Manney, G., Luo, B., Arfeuille, F., and Peter, T.: A global space-based stratospheric aerosol climatology: 1979–2016, Earth System Science Data, 10, 469–492, https://doi.org/10.5194/essd-10-469-2018, 2018.

Thomason, L. W., Kovilakam, M., Schmidt, A., von Savigny, C., Knepp, T., and Rieger, L.: Evidence for the predictability of changes in the stratospheric aerosol size following volcanic eruptions of diverse magnitudes using space-based instruments, Atmospheric Chemistry and Physics, 21, 1143–1158, https://doi.org/10.5194/acp-21-1143-2021, 2021.

Vernier, J.-P., Thomason, L., Pommereau, J.-P., Bourassa, A., Pelon, J., Garnier, A., Hauchecorne, A., Blanot, L., Trepte, C., Degenstein, D., et al.: Major influence of tropical volcanic eruptions on the stratospheric aerosol layer during the last decade, Geophys. Res. Lett., 38, 2011.

Vernier, J.-P., Fairlie, T., et al.: Increase in upper tropospheric and lower stratospheric aerosol levels and its potential connection with Asian Pollution, J. Geophys. Res. Atmos., 120, 1608–1619, 2015.

Wang, H. J. R., Damadeo, R., Flittner, D., Kramarova, N., Taha, G., Davis, S., Thompson, A. M., Strahan, S., Wang, Y., Froidevaux, L., Degenstein, D., Bourassa, A., Steinbrecht, W., Walker, K. A., Querel, R., Leblanc, T., Godin-Beekmann, S., Hurst, D., and Hall, E.: Validation of SAGE III/ISS Solar Occultation Ozone Products With Correlative Satellite and Ground-Based Measurements, Journal of Geophysical Research: Atmospheres, 125, e2020JD032 430, https://doi.org/https://doi.org/10.1029/2020JD032430, e2020JD032430 2020JD032430, 2020.

Wang, P.-H., McCormick, M., Poole, L., Chu, W., Yue, G., Kent, G., and Skeens, K.: Tropical high cloud characteristics derived from SAGE II extinction measurements, Atmospheric Research, 34, 53–83, https://doi.org/https://doi.org/10.1016/0169-8095(94)90081-7, 11th conference on clouds and precipitation, 1994.

Xian, T. and Homeyer, C. R.: Global tropopause altitudes in radiosondes and reanalyses, Atmospheric Chemistry and Physics, 19, 5661–5678, https://doi.org/10.5194/acp-19-5661-2019, 2019.

Yu, P., Toon, O. B., Bardeen, C. G., Zhu, Y., Rosenlof, K. H., Portmann, R. W., Thornberry, T. D., Gao, R.-S., Davis, S. M., Wolf, E. T., de Gouw, J., Peterson, D. A., Fromm, M. D., and Robock, A.: Black carbon lofts wildfire smoke high into the stratosphere to form a persistent plume, Science, 365, 587–590, https://doi.org/10.1126/science.aax1748, 2019.

A sample extinction profile at 756 nm that shows how negative extinction values in the lower stratosphere as well as in the troposphere (Left). The right panel shows the extinction profile after filtering negative values. Red, and blue symbols in the left panel shows negative extinction values with uncertainty $> 50\%$ and $< 50\%$ respectively, while orange symbols represent positive extinction with $> 50\%$ uncertainty. The absolute value of the negative extinction coefficients (blue and red dots) are plotted to accommodate the log scale.

Extinction efficiency as a function radius for all SAGE III/ISS wavelengths (a) and radius versus extinction ratios (b).

Scatter plots of 756 to 1544 nm extinction ratio as a function of 1544 nm extinction at 15 km altitude for February for the time period between 2017 and 2021, using TV13 Method. (a) before filtering and (b) after filtering.

Time series of k_0 1544 nm extinction for different latitude bands. Red symbols show the time line of enhanced aerosol extinction coefficient and the time it takes to get back to the background aerosol level following each event. The panels show events listed in Table 1 with (a) Canadian Wildfire, (b) Ambae eruption, (c) Ulawun Eruption, (d) Raikoke Eruption, (e) Australian Wildfire, (f) California Creek Fire, (g) La Soufriere and (h) McKay Creek Fire.

Scatter plots of 756 to 1544 nm extinction ratio versus 1544 nm extinction following Canadian Wildfire event in 201708 and Ambae eruption in 201807.

Scatter plots of 756 to 1544 nm extinction ratio versus 1544 nm extinction following Canadian Wildfire event in 201708 (a-d) and Ambae eruption in 201807 (e-h), after applying cloud/aerosol categorization.

Scatter plots of 756 to 1544 nm extinction ratio as a function of 1544 nm extinction at 11 and 16km for the time period between 2017 and 2021, after filtering out possible aerosol/cloud mixture. (a,c) TV13 Method and (b,d) New Method.

Zonally averaged SAGE III/ISS altitude versus latitude extinction coefficient plot for September 2017 following Canadian wildfire event. (a) version 5.1 (b) for version 5.2 and (c) ratio between version 5.2 and 5.1. Extinction coefficient values are shown in the log base to the 10.

Altitude versus Latitude of Ångström exponent monthly climatology derived using OSIRIS 750 nm and SAGE II and SAGE III/ISS 525 nm extinction. Outliers are removed using 3x3 median smoothing. Please note that we apply linear interpolation to fill in missing data that are mostly applicable for the polar latitude (poleward of 55).

Percent difference between OSIRIS and SAGE III/ISS altitude versus latitude for June 2017 (a) at 525 nm , and (b) 750 nm. Ångström exponent of 2.33 is used to convert OSIRIS extinction to 525 nm in (a) while a monthly climatology of Ångström exponent from Figure 6 is used to convert OSIRIS extinction in (c).

Percent difference between CALIOP, bias corrected OSIRIS, and cloud screened SAGE III/ISS extinction coefficients for November 2017. CALIOP data used in (a) and (b) are for 532 nm available in CALIOP stratospheric aerosol product, whereas CALIOP data in (c) and (d) are bias corrected using the scale factor (SF) showed in Figure 9a.

Altitude versus latitude dependence of 525 bias corrected OSIRIS extinction to 532 CALIOP backscatter ratio (SF) for the overlap period between 2006 and 2020.

Altitude versus latitude dependence of 525 nm extinction for September 2017 and August 2018. (a) for GloSSAC version 2.0, (b) for GloSSAC version 2.2, and (c) ratio between version 2.2 and 2.0. Lower panels show same as in the upper panel but for August 2018.

Altitude versus latitude dependence of 525 nm extinction for September 2017. (a,c,e,g) for OSIRIS, CALIPSO, SAGE III/ISS, and merged extinction for version 2.0 respectively whereas (b,d,f,h) are for version 2.2. (i) shows the ratio between merged version 2.2 and 2.0.

Latitude versus time dependence of SAOD for 525 and 1020 nm. (a,b,c) SAOD for 525 nm for GloSSAC version 2.0, version 2.2, and percent difference between (a) and (b). (d,e,f) Same as in (a,b,c) but for 1020 nm. (b, e) show major volcanic eruptions (black) and wild fire events (green) with abbreviated two letter code with their respective latitude and time of occurrence that are listed here. The event names shown in figures are: St. Helens (He), El Chichon (El), Nevado del Ruiz (Ne), Kelut (Ke), Pinatubo (Pi), Mt. Hudson (Ce),Rabaul (Ra), Manam (Mn), Soufriere Hills (So), Tavurvur (Tv), Chaiten (Ch), Okmok (Ok), Kasatochi (Ka), Sarychev (Sv), Nabro (Nb), Kelut (Ke), Calbuco (Cb), Canadian Wildfires (Cw), Ambae (Am), Ulawun (Ul), Australian Wildfire (Aw), California Creek Fire (Cc), La Soufriere (La), McKay Creek Fire (Mc).

Time series of globally averaged SAOD for 525 and 1020 nm. Percent difference between version 2.0 and 2.2 are shown in (b,d) for 525 and 1020 nm.

Volcanic and PyroCb events used in this study

Event Name Event Date Latitude

Canadian Wildfire (Cw) 17 July 2017 51N Ambae Eruption (Am) 28 July 2018 15S Ulawun Eruption (Ul) 22 June 2019 5S Raikoke Eruption (Ra) 03 August 2019 48NAustralian Wildfire (Aw) 06 January 2020 34S California Creek Fire (Cc) 01 September 2020 37NLa Soufriere (La) 22 April 2021 13NMcKay Creek Fire (Mc) 29 June 2021 54N